Classic cadherins mediate selective intracortical circuit formation in the mouse neocortex

Classic cadherins mediate selective intracortical circuit formation in the mouse neocortex

Mayu Wakimoto[1,2,3], Keisuke Sehara[3], Haruka Ebisu[1,2,3], Yoshio Hoshiba[1,2,3], Shinichi Tsunoda[1,2], Yoshie Ichikawa[1,2] and Hiroshi Kawasaki[1,2,3]

[1] Department of Biophysical Genetics, Graduate School of Medical Sciences, Kanazawa University, Ishikawa 920-8640, Japan

[2] Brain/Liver Interface Medicine Research Center, Kanazawa University, Ishikawa 920-8640, Japan

[3] Department of Molecular and Systems Neurobiology, Graduate School of Medicine, The University of Tokyo, Tokyo 113-0033, Japan

Address correspondence to
Hiroshi Kawasaki, MD, PhD
Department of Biophysical Genetics
Graduate School of Medical Sciences
Kanazawa University
Takara-machi 13-1, Kanazawa, Ishikawa 920-8640, Japan
Tel: +81-76-265-2363
Fax: +81-76-234-4728
E-mail: hiroshi-kawasaki@umin.ac.jp

Abstract

Understanding the molecular mechanisms underlying the formation of selective intracortical circuitry is one of the important questions in neuroscience research. "Barrel nets" are recently identified intracortical axonal trajectories derived from layer 2/3 neurons in layer 4 of the primary somatosensory (barrel) cortex. Axons of layer 2/3 neurons are preferentially distributed in the septal regions of layer 4 of the barrel cortex, where they show whisker-related patterns. Because cadherins have been viewed as potential candidates that mediate the formation of selective neuronal circuits, here we examined the role of cadherins in the formation of barrel nets. We disrupted the function of cadherins by expressing dominant-negative cadherin (dn-cadherin) using *in utero* electroporation and found that barrel nets were severely disrupted. Confocal microscopic analysis revealed that expression of dn-cadherin reduced the density of axons in septal regions in layer 4 of the barrel cortex. We also found that cadherins were important for the formation, rather than the maintenance, of barrel nets. Our results uncover an important role of cadherins in the formation of local intracortical circuitry in the neocortex.

Keywords: barrel nets, intracortical circuit, *in utero* electroporation, layer 2/3 neurons, somatosensory cortex

Introduction

The cerebral cortex contains complex and sophisticated neuronal circuitries that are the structural bases of higher brain functions. Because the formation of appropriate neuronal circuitry in the cerebral cortex during development is essential for normal brain functions, it is important to elucidate the mechanisms underlying the formation of neuronal circuitry in the cerebral cortex. Although previous pioneering studies have intensively investigated the electrophysiological and anatomical properties of local neuronal circuitry in the cerebral cortex, the mechanisms underlying the formation of local neuronal circuitry in the cerebral cortex are not fully understood.

The primary somatosensory cortex (barrel cortex, S1) has been widely used for investigating neural circuits and the mechanisms underlying their formation (Woolsey 1990; O'Leary et al. 1994; Erzurumlu and Kind 2001; López-Bendito and Molnár 2003; Rebsam and Gaspar 2006; Fox 2008; Toda et al. 2008; Meyer et al. 2010a; Meyer et al. 2010b; Erzurumlu and Gaspar 2012; Oberlaender et al. 2012; Toda et al. 2013). Using *in utero* electroporation as a tool to visualize axonal trajectories of a selective population of cortical neurons, we recently uncovered a novel intracortical circuit, which we named "barrel nets", in layer 4 of the barrel cortex in mice and rats; axons of layer 2/3 neurons are predominantly located in the septal regions of layer 4 and therefore show a whisker-related pattern (Sehara et al. 2010; Sehara and Kawasaki 2011; Sehara et al. 2012). Our results showing presynaptic structures on barrel nets suggested that barrel nets are involved in the functioning of the neuronal circuitry of the barrel cortex (Sehara et al. 2010; Sehara et al. 2012).

To investigate the mechanisms underlying the formation of intracortical neural circuits, we focused on classic cadherins, which are known as homophilic cell adhesion

molecules (Takeichi 1991; Redies and Takeichi 1996; Tepass et al. 2000; Takeichi 2007). This was because it has been proposed that the homophilic binding activity of classic cadherins is well suited to mediate selective circuit formation (Suzuki et al. 1997; Inoue et al. 1998). Furthermore, it has been reported that several classic cadherins are predominantly expressed in whisker-related patterns in the barrel cortex. *Cadherin-8* mRNA was detected in septal regions of layer 4, as well as layers 2/3 and 5a (Suzuki et al. 1997; Gil et al. 2002; Dye et al. 2011; Hertel and Redies 2011; Krishna-K et al. 2011; Lefkovics et al. 2012). Previous studies showed that, in the developing barrel cortex, *cadherin-6* expression is relatively high in septal regions compared to barrel hollows (Suzuki et al. 1997; Inoue et al. 2008; Krishna-K et al. 2011; Lefkovics et al. 2012; Terakawa et al. 2013). In addition, immunohistochemical studies revealed that R-cadherin and N-cadherin expressions are observed in barrel hollows of layer 4 (Huntley and Benson 1999; Obst-Pernberg et al. 2001). However, the roles of classic cadherins in selective circuit formation in the cerebral cortex still remained largely elusive. Here, using barrel nets as a model, we uncovered a role of classic cadherins in intracortical circuit formation.

Materials and Methods

Animals

ICR mice were purchased from SLC (Hamamatsu, Japan) and were reared on a normal 12 h light/dark schedule. The day of conception and that of birth were counted as E0 and P0, respectively. All procedures were performed in accordance with protocols approved by the University of Tokyo Animal Care Committee and Kanazawa University Animal Care

Committee. All experiments were repeated at least three times and gave consistent results.

Plasmids

All genes were expressed under the control of the CAG promoter (Niwa et al. 1991). Plasmids were purified using the EndoFree plasmid maxi kit (QIAGEN, Germany). pCAG-GFP, pCAG-mCherry and pCAG-synaptophysin-GFP were described previously (Sehara et al. 2010). Dominant-negative cadherins, hDNcad and cN390Δ, were generous gifts from Dr. Jonas Frisén (Karolinska Institutet, Sweden) and Dr. Masatoshi Takeichi (RIKEN CDB, Japan), respectively (Fujimori and Takeichi 1993; Nieman et al. 1999; Togashi et al. 2002; Barnabé-Heider et al. 2008). pCAG-hDNcad and pCAG-cN390Δ were made by substituting GFP of pCAG-GFP with hDNcad and cN390Δ, respectively. pCAG-synaptophysin-mCherry was made by substituting GFP of pCAG-synaptophysin-GFP with mCherry. pCAG-$ER^{T2}CreER^{T2}$ and pCAG-floxedSTOP-GFP were described previously (Ako et al. 2011). pCAG-floxedSTOP-mCherry, pCAG-floxedSTOP-hDNcad and pCAG-floxedSTOP-cN390Δ were made by replacing GFP of pCAG-floxedSTOP-GFP with mCherry, hDNcad and cN390Δ, respectively.

In utero *electroporation*

In utero electroporation was performed as described previously with slight modifications (Sehara et al. 2010; Kawasaki et al. 2012; Kawasaki et al. 2013). Briefly, pregnant animals were anesthetized with sodium pentobarbital, and the uterine horns were exposed. Approximately 1-2 μl of DNA solution (1-3 mg/ml) was injected into the lateral ventricle of embryos at the indicated ages using a pulled glass micropipette. Each embryo within the uterus was placed between tweezer-type electrodes (CUY650-P5, NEPA Gene, Japan). Square

electric pulses (45 V, 50 ms) were passed five times at 1 s intervals using an electroporator (ECM830, Harvard Apparatus, USA). The directions of pulses were adjusted so that cortical glutamatergic neurons were transfected. Care was taken to quickly place embryos back into the abdominal cavity to avoid excessive temperature loss. The wall and skin of the abdominal cavity were sutured, and embryos were allowed to develop normally.

4-hydroxytamoxifen (4-OHT) administration

4-OHT (>70% Z isomer, Sigma-Aldrich, St. Louis, USA) administration was performed as described previously with slight modifications (Ako et al. 2011). 4-OHT was dissolved in 99.5% EtOH at a concentration of 20 mg/ml as stock solution. The stock solution was diluted with sesame oil at a concentration of 2 mg/ml before use, and then the EtOH was vaporized. 4-OHT in sesame oil was injected subcutaneously 66 μg/g body weight at the indicated time points.

Dissociated primary cultures of cortical neurons

Cultures of dissociated cortical neurons were made as described previously with slight modifications (Yamasaki et al. 2011). *In utero* electroporation was performed at E15.5, and the cerebral cortex was dissected at E16.5. After the meninges were pulled off, the dissected cortices were incubated for 20 min in papain solution plus DNase I at 37°C, and were dissociated mechanically. The dissociated neurons were plated onto poly-D-lysine-coated coverslips in 24 well plate ($1x10^6$ cells/well), and maintained in 50% Basal Medium Eagle (Invitrogen) containing 1 mM L-glutamine (Sigma-Aldrich), 25% Hank's balanced salt solution (Invitrogen), 25% horse serum (Invitrogen), 6.5 mg/ml D-glucose (Sigma-Aldrich), 100 U/ml penicillin/streptomycin (Invitrogen), and 1% HEPES pH 7.4 (Invitrogen) at 37°C in

5% CO_2. The day of dissection was counted as day *in vitro* 0 (DIV0).

Immunohistochemistry and immunocytochemistry

Immunohistochemistry was performed as described previously (Toda et al. 2008; Hayakawa and Kawasaki 2010; Iwai et al. 2013). Briefly, mice were anesthetized with pentobarbital and transcardially perfused with 4% paraformaldehyde/PBS. To make coronal sections, the cerebral cortices were dissected, cryoprotected by overnight immersion in 30% sucrose/PBS, and embedded in OCT compound. To make tangential sections, the cortical hemispheres were isolated, flattened and embedded in OCT compound as described previously (Toda et al. 2008; Sehara et al. 2010). Sections were made using a cryostat.

Sections of 50 μm thickness were permeabilized with 0.1–0.5% Triton X-100 in PBS and incubated overnight with primary antibodies. After being incubated with Alexa 488-, Alexa 647- or Cy3- conjugated secondary antibodies and 1 μg/ml Hoechst 33342, the sections were washed and mounted. The primary antibodies included rabbit anti-VGLUT2 antibody (Synaptic Systems, Germany), goat anti-VGLUT2 antibody (Frontier Institute, Japan), rabbit anti-GFP antibody (Medical & Biological Laboratories, Japan), rat anti-GFP antibody (Nacalai Tesque, Japan), rabbit anti-RFP antibody (Medical & Biological Laboratories, Japan), rabbit anti-RORβ antibody (Diagenode, USA), goat anti-Brn2 antibody (Santa Cruz, USA), and rat anti-Ctip2 antibody (Abcam, USA).

For immunocytochemistry, dissociated neurons cultured on coverslips were fixed with 4% paraformaldehyde/PBS for 15 min at 37°C. Then, the neurons were incubated in blocking solution (2% BSA/PBS), and were incubated at 4°C overnight with primary antibodies, which included rat anti-GFP antibody (Nacalai Tesque, Japan) and sheep anti-N-cadherin antibody (R&D Systems). The neurons were washed with 0.5% Triton

X-100/PBS and then incubated with Alexa488- and Cy3-conjugated secondary antibodies and 1 µg/ml Hoechst 33342, followed by washing and mounting.

In situ *hybridization*

In situ hybridization was performed as described previously with slight modifications (Kawasaki et al. 2004; Iwai and Kawasaki 2009). Sections with 25 µm thickness were prepared from fresh-frozen tissues, and those with 14 µm thickness were from fixed tissues. The sections were treated with 4% paraformaldehyde for 10 min and 0.25% acetic anhydride for 10 min. After prehybridization, the sections were incubated overnight at 58°C with digoxigenin-labeled RNA probes for *cadherin-6, cadherin-8* or *hDNcad* diluted in hybridization buffer (50% formamide, 5×SSC, 5×Denhardt's solution, 0.3 mg/ml yeast RNA, 0.1 mg/ml herring sperm DNA, and 1 mM DTT). The sections were washed with SSC, incubated with alkaline phosphatase-conjugated anti-digoxigenin antibody (Roche), and then incubated with NBT/BCIP as substrates.

Microscopy

Epifluorescence microscopy was performed with an AxioImager A1 microscope (Carl Zeiss, Germany) or a BIOREVO BZ-9000 (Keyence, Japan). Confocal microscopy was performed with an LSM510 microscope (Carl Zeiss, Germany) or an FV10i FLUOVIEW microscope (OLYMPUS, Japan).

Quantifications of barrel net formation

Quantifying GFP fluorescence of barrel nets was performed as described previously (Sehara et al. 2010). Briefly, coronal sections of 50 µm thickness were prepared at the indicated time

points and stained using VGLUT2 antibody. Images were taken under a confocal microscope. Signals in layer 4 were measured using the "Plot Profile" command of ImageJ (NIH). Each barrel unit (which refers to a barrel and its septal rim) was then separated using VGLUT2 signal intensities in layer 4. GFP signals within each barrel unit were normalized by subtracting the minimum value within the barrel unit from the measured values, and dividing the values by the total signal intensity of the barrel unit. Each barrel unit was divided into ten subunits of equal width (hereafter referred to as barrel subunits), and the values of each subunit were plotted against the horizontal position of the subunit within the barrel unit.

To calculate the periphery/center ratio (p/c ratio) for GFP, the mean signal intensity of subunits 1 and 10 was divided by that of subunits 5 and 6. The center/periphery ratio (c/p ratio) of VGLUT2 was the inverse number of the p/c ratio. For statistical analyses of the p/c and c/p ratio, the average value was calculated for each pup and compared using Welch's *t*-test.

Quantification of the morphology of dissociated neurons

Dissociated primary cultures were fixed at DIV4 and were stained with anti-GFP antibody. Images were taken under an epifluorescence microscope, and axons from individual neurons were traced using the NeuronJ plugin (Meijering et al. 2004; Meijering 2010) of ImageJ software. We used the "Add tracings" command for tracing the axons and the "Measure tracings" command for measuring the length of axon branches in NeuronJ. Branch patterns were annotated manually using NeuronJ, and then the analysis and statistics were performed using the R environment (R Core Team. 2014). Five GFP-positive neurons on each coverslip were traced and analyzed. Seven coverslips per each experimental condition were used for statistical analyses using Welch's *t*-test.

Quantifications of the expression of layer markers and the density of GFP-positive neurons

Z-stack images of immunostained sections were taken using a confocal microscope, and the expression of layer markers was examined in GFP-positive neurons with Hoechst-positive nuclei. GFP-positive neurons without Hoechst-positive nuclei were excluded from the analyses.

To determine the transfection efficiency, the density of GFP-positive neurons in layer 2/3 of coronal sections with 50 μm thickness was calculated. Statistical analyses were performed using Mann-Whitney's *U*-test.

Quantifications of the density and the size of synaptophysin-mCherry-postive puncta

Coronal sections prepared at P15 were immunostained, and *Z*-stack confocal images were taken. Average-projection images with 3.5 μm optical thickness were smoothened (mean filter, 2 μm radius) and then used for further analyses. Synaptophysin-mCherry positive puncta were detected using the "Find maxima" command of ImageJ, in which mean plus standard deviation values were used as the tolerance level. GFP-positive axons were traced, and their lengths were measured using the original images and NeuronJ. Then, mCherry-positive puncta were counted only if they overlapped with GFP-positive axons. The radius of mCherry-positive puncta was calculated as the distance from the maxima to the first deflection point of the mCherry fluorescence. Mann-Whitney's *U*-test was used for statistical analyses.

Results

ER^{T2}Cre-mediated postnatal expression of dominant-negative cadherin in layer 2/3 neurons

Because it has been reported that the multiple classic cadherins are expressed in whisker-related patterns in the somatosensory cortex (See also Supplementary Fig. 1) (Huntley and Benson 1999; Obst-Pernberg et al. 2001; Huntley 2002; Dye et al. 2011; Krishna-K et al. 2011), we simultaneously suppressed functions of multiple classic cadherins using dominant-negative cadherin (dn-cadherin). Consistent with a previous report (Nieman et al. 1999), our experiments using dissociated primary cultures of the cerebral cortex demonstrated that the dn-cadherin hDNcad (Nieman et al. 1999; Barnabé-Heider et al. 2008) strongly inhibited the expression of classic cadherins in cortical layer 2/3 neurons (Supplementary Fig. 2). We then co-expressed GFP and hDNcad in layer 2/3 neurons *in vivo* using *in utero* electroporation at E15.5 under the control of the CAG promoter. Consistent with a previous report (Kawauchi et al. 2010), however, constitutive expression of hDNcad disrupted migration of the GFP-positive transfected layer 2/3 neurons (Fig. 1*A*).

To avoid the migration defects caused by dn-cadherin, we used the ER^{T2}Cre/loxP system to control the timing of dn-cadherin expression (Fig. 1*B*) (Matsuda and Cepko 2007). We transfected layer 2/3 neurons with pCAG-ER^{T2}CreER^{T2}, pCAG-floxedSTOP-XFP and pCAG-floxedSTOP-hDNcad using *in utero* electroporation at E15.5 and examined the time point after which 4-hydroxytamoxifen (4-OHT) injection does not lead to the migration defect (Fig. 1*B*, *C*). While injection of 4-OHT at P0 caused the evident migration defect (Fig. 1*C*, arrowheads), injection at or after P2 did not (Fig. 1*C*). We therefore injected 4-OHT at P2 in the following experiments.

Next, we examined how many times of 4-OHT injection are necessary for sufficient ER^{T2}Cre-mediated gene expression (Fig. 2). Expression levels of GFP and the number of

GFP-positive cells were markedly increased in samples that received 4-OHT injection daily for three consecutive days than in those that received injection only once (Fig. 2*B*). Therefore, to sufficiently express dn-cadherin only after migration of layer 2/3 neurons had occurred, we injected 4-OHT daily from P2 to P4 in the following experiments.

Postnatal expression of dn-cadherin in layer 2/3 neurons disrupted barrel nets in the barrel cortex

We then examined if classic cadherins are required for the formation of barrel nets by expressing dn-cadherin and GFP in layer 2/3 neurons (Fig. 3*A*). Although the whisker-related pattern of barrel nets was clearly visible in tangential sections of control samples, we found that the pattern was almost absent in samples expressing hDNcad (Fig. 3*B*). To make sure that this effect of hDNcad is mediated by suppressing cadherin functions, we employed another dn-cadherin, cN390Δ (Fujimori and Takeichi 1993; Togashi et al. 2002). Consistently, we found that the expression of cN390Δ also resulted in disruption of barrel nets (Fig. 3*C*). Examination using coronal sections also showed that GFP-positive axons failed to accumulate in septal regions of layer 4 when one of the dn-cadherin constructs was expressed in layer 2/3 (Fig. 4*A*, hDNcad and cN390Δ). These results suggest that inhibition of classic cadherin functions in layer 2/3 neurons disrupts the formation of the barrel net pattern.

We then quantified the effect of dn-cadherin on barrel net formation with a method we used previously (Sehara et al. 2010). We quantified the distribution of GFP-positive axons around individual barrels in coronal sections using confocal microscopic images (Supplementary Fig. 3). In control samples, GFP-positive axons were abundant in peripheral regions around thalamocortical axon patches visualized by anti-VGLUT2 antibody (Supplementary Fig. 3, control. Compare green and gray) (Fremeau et al. 2001; Fujiyama et al.

2001). In contrast, in dn-cadherin samples, such preferential distribution of GFP-positive axons was inhibited (Supplementary Fig. 3, hDNcad, green). We calculated the ratio of GFP signal intensities in peripheral regions to those in central regions of individual VGLUT2-positive patches (hereafter referred to as "the periphery/center ratio" or "the p/c ratio". See Materials and Methods for details) (Fig. 4*B*, green). We found that the p/c ratio of GFP was significantly higher in control samples than that in dn-cadherin samples (Fig. 4*B*, green), while the c/p ratio of VGLUT2 signals was similar in both control and dn-cadherin samples (n = 3 pups for each condition from 3 pregnant mice). However, the density of GFP-positive layer 2/3 neurons in hDNcad samples was not different from that in control samples (Fig. 4*D*) (n = 3 pups for each condition from 3 pregnant mice). Taken together, these results indicate that classic cadherins play a crucial role in the formation of barrel nets.

Classic cadherins are required for the accumulation of fine axons in septal regions

Because our previous confocal microscopic studies showed that there is a much higher density of GFP-positive fine axon branches in septa than in barrel hollows (Sehara et al. 2010; Sehara et al. 2012), it seemed plausible that the effect of dn-cadherin on barrel nets resulted from the reduction of fine axons in the septal regions of layer 4. We therefore examined the phenotype of dn-cadherin overexpression in more detail using a confocal microscope (Fig. 4*C*). We found that the number of fine axon branches markedly decreased in septal regions when hDNcad was expressed (Fig. 4*C*). Although hDNcad samples may have more axons in the barrel hollows, it was difficult to conclude whether hDNcad affected the number of axons in the barrel hollows. These results indicate that classic cadherins are required for the accumulation of fine axons in the septal regions of layer 4.

Because previous studies reported that classic cadherins are involved in axonal

elongation of retinal ganglion cells (Riehl et al. 1996), it was possible that the effect of dn-cadherin on barrel nets was just a result of a general defect in the axonal elongation of transfected layer 2/3 neurons. In order to address if dn-cadherin expression affects axon elongation in general, we examined the extent of callosal axon projection from layer 2/3 neurons (Fig. 5). Notably, layer 2/3 neurons, regardless of whether they were transfected with hDNcad or control vectors, sent callosal axons to a similar extent in the contralateral cortex, suggesting that the defect in the formation of barrel nets in dn-cadherin samples is not simply because of the inhibition of axonal elongation in general.

It seemed intriguing to examine the effects of dn-cadherin on the morphology of the axons of layer 2/3 neurons at the single-cell level. We therefore transfected layer 2/3 neurons with pCAG-GFP plus either pCAG-hDNcad or a control plasmid, and made dissociated primary cultures of the cerebral cortex (Fig. 6). Although we quantified several parameters of the morphology of axons such as the number of branches per an axon (Fig. 6*B*), the total length of each axon (Fig. 6*C*) and the length of individual axonal branches (Fig. 6*D*, *E*), none of these parameters were significantly different between control and hDNcad-transfected neurons (n = 7 coverslips for each condition). These results imply that dn-cadherin affects the location of axonal branches but not the branching or elongation of axons.

Although dn-cadherin-expressing layer 2/3 neurons were located in the appropriate layer (i.e. layer 2/3), it seemed still possible that the expression of dn-cadherin affected the layer identities of transfected layer 2/3 neurons, and as a result, the pattern of barrel nets was disrupted. To address this point, we performed immunohistochemistry using antibodies against layer marker proteins (Fig. 7). We used Brn2, which is predominantly expressed in layers 2/3 and 5, and Ctip2, which is a marker for layers 5–6 (Hevner et al. 2003; Arlotta et al. 2005). We also used RORβ, which is mainly expressed in layer 4 and sparsely in layer 5

(Schaeren-Wiemers et al. 1997; Nakagawa and O'Leary 2003). Higher magnification images showed that Brn2, RORβ and Ctip2 immunoreactivities were located in the nucleus (Fig. 7*D, E*). We found that expression patterns of the layer markers in hDNcad samples were indistinguishable from those in the control samples (Fig. 7*A-C*). In addition, our quantification also revealed that GFP-positive cells in the hDNcad samples had similar expression profiles to those in control samples (Fig. 7*C*; n = 3 pups for each condition from 5 pregnant mice). These data suggest that postnatal overexpression of dn-cadherin does not affect the layer identities of transfected layer 2/3 neurons, but specifically alters the regional selectivity of axon distribution in layer 4 of the barrel cortex.

Postnatal dn-cadherin expression decreased presynaptic structures in septal regions

Because our previous studies have suggested that barrel nets contain presynaptic structures (Sehara et al. 2010; Sehara et al. 2012), we next examined whether the expression of dn-cadherin affects the number of synaptic structures on barrel nets. We examined the distribution of presynaptic structures on barrel nets, using XFP-tagged synaptophysin as a presynaptic marker (Sehara et al. 2010; Sehara et al. 2012).

First, we examined the developmental time course of the formation of presynaptic structures on barrel nets. We expressed mCherry and synaptophysin-GFP in layer 2/3 neurons and examined the distribution patterns of GFP-positive puncta on mCherry-positive barrel nets during development (Fig. 8*A*). Synaptophysin-GFP-positive puncta markedly increased between P5 and P15, corresponding to the increase of mCherry-positive axons in septal regions (Fig. 8*A*). We found that the number of synaptophysin-mCherry puncta was markedly reduced by hDNcad, suggesting that dn-cadherin expression affects not only the distribution of axons but also the number of presynaptic structures on barrel nets (Fig. 8*B*). Our

quantification of mCherry-positive puncta on GFP-positive axons showed that neither their density (i.e. the number of mCherry-positive puncta per unit axon length) nor the size of individual mCherry-positive puncta was affected by hDNcad expression (Fig. 8*C-E*; n = 3 pups for each condition from 4 pregnant mice). This result suggests that, although the number of mCherry-positive puncta was reduced by hDNcad, this reduction is due to the decrease in the number of axons in the septal region.

Classic cadherins are required for the formation, but not for the maintenance, of barrel nets

So far, our results were consistent with the idea that classic cadherins are required for the formation of barrel nets. On the other hand, it still remained possible that classic cadherins are involved in the maintenance, rather than the formation, of the pattern of barrel nets. However, we believe that this is unlikely because of the following two reasons. The first reason is that barrel nets did not appear from the beginning when dn-cadherin was expressed. We examined the effect of hDNcad sequentially at P5, P10 and P15 (Fig. 9*A*). In control animals, barrel nets were invisible at P5 and were formed gradually thereafter as we reported previously (Sehara et al. 2010). Interestingly, in hDNcad-transfected animals, barrel nets never appeared (Fig. 9*B*), suggesting that the formation of barrel nets was inhibited.

The second reason is the fact that expression of dn-cadherin after the formation of barrel nets did not disrupt barrel net patterns. We expressed hDNcad after the formation of barrel nets by late administration of 4-OHT and examined if the late expression of dn-cadherin results in the degradation of barrel nets (Fig. 9*C*). Interestingly, the expression of hDNcad after the formation of barrel nets did not disrupt barrel nets (Fig. 9*D*, late 4-OHT), while hDNcad expression before the formation of barrel nets effectively disrupted barrel nets

(Fig. 9*D*, early 4-OHT). Our quantification using confocal microscopic images also supported this conclusion (early 4-OHT, control, n = 3 pups; early 4-OHT, hDNcad, n = 3 pups; late 4-OHT, control, n = 4 pups; late 4-OHT, hDNcad, n = 3 pups; from 4 pregnant mice) (Fig. 9*E*). Because it seemed possible that late 4-OHT treatment failed to induce hDNcad, we examined if hDNcad expression was indeed induced by late 4-OHT treatment by using *in situ* hybridization. We made an *in situ* hybridization probe which detects hDNcad but does not detect endogenous mouse cadherins in the barrel cortex (Supplementary Fig. 4*A*, *B*). Our late 4-OHT treatment led to strong hDNcad expression, as in the case of early 4-OHT treatment (Supplementary Fig. 4*B*). Collectively, our results suggest that classic cadherins are required for the formation, rather than the maintenance, of barrel nets.

Discussion

Here we have shown that classic cadherins are required for the formation, rather than the maintenance, of local circuits in the cerebral cortex during development. Elongation of callosal axons derived from layer 2/3 neurons was not affected by dn-cadherin, suggesting that dn-cadherin selectively inhibited barrel net formation. Our results suggest that classic cadherins are also important for the development of presynaptic structures on barrel net axons. Our findings uncovered an important role of classic cadherins in local intracortical circuit formation.

Because previous reports showed multiple classic cadherins are expressed in whisker-related patterns (Huntley and Benson 1999; Obst-Pernberg et al. 2001; Huntley 2002; Dye et al. 2011; Krishna-K et al. 2011), we utilized dn-cadherin to suppress these classic cadherins simultaneously and uncovered that classic cadherins are indeed required for barrel

net formation. In order to fully understand the cadherin-mediated mechanisms underlying barrel net formation, there are several important questions to be addressed. First, it would be important to investigate which of the classic cadherins mediate barrel net formation. Combining cadherin-knockout mice and *in utero* electroporation to reveal barrel nets would be appropriate experiments to address this point. Second, because classic cadherins mediate homophilic binding, it seems possible that cadherin molecules on barrel net axons bind to cadherin molecules expressed on other cells in the septa. It would be intriguing to investigate which neurons in which layers are responsible for this. Alternatively, it seems also possible that cadherins on axons in barrel nets bind to cadherins on neighboring axons in the same barrel net. Third, it would be intriguing to examine the effect of dn-cadherin at the level of single axons. When GFP is expressed with conventional *in utero* electroporation, numerous axons in barrel nets are labeled with GFP, and as a result, it is difficult to examine what happens to individual GFP-positive axons, such as branching, elimination and elongation. Our experiments using dissociated primary cultures showed that axon elongation and branching were not affected by dn-cadherin *in vitro*. Therefore, it seems reasonable to speculate that GFP-positive axons in septal regions were shifted into barrel hollows by hDNcad expression, though this should be addressed by future detailed morphological analyses of single neurons *in vivo*. Future experiments would be required for obtaining a complete understanding of the mechanisms underlying barrel net formation.

Because of their homophilic binding activity and intriguing expression patterns, classic cadherins have been proposed to be key molecules in the regulation of selective neuronal circuit formation (Suzuki et al. 1997; Inoue et al. 1998). A recent report showed that cadherin-6 mediates axon-target matching of retinal ganglion cell axons in the visual thalamus (Osterhout et al. 2011). Another report demonstrated that cadherin-9 regulates

synapse-specific differentiation in the hippocampus (Williams et al. 2011). However, involvement of classic cadherins in selective local circuit formation in the neocortex has not been well understood. Our results indicate that classic cadherins indeed mediate selective local circuit formation in the neocortex. It remains unclear how cadherins actually regulate selective circuit formation in barrel nets. As discussed above, it seems likely that the homophilic binding activity of cadherins is involved in axon guidance. On the other hand, it seems also possible that cadherins primarily regulate synaptogenesis to stabilize the distribution of axons because previous studies showed that cadherins are important for synaptogenesis (Togashi et al. 2002; Bozdagi et al. 2004; Williams et al. 2011). However, we think that the latter is unlikely for barrel nets because we showed that the density of synapses along individual axons was not affected by expressing dn-cadherin. It would be intriguing to examine the differential roles of cadherins in axon formation and synaptogenesis.

Uncovering the mechanisms underlying the formation of local intracortical circuits would lead to a better understanding of the development and function of the cerebral cortex. Although we have uncovered anatomical structures and developmental processes of barrel nets (Sehara et al. 2010; Sehara et al. 2012), the function of barrel nets still remains unknown. It seems appropriate to speculate that the function of barrel nets is suppressed in dn-cadherin-expressing animals because of the severe reduction in the number of presynaptic structures by dn-cadherin. Further understanding of the mechanisms underlying barrel net formation would lead to selective loss-of-function experiments involving barrel nets such as the generation of animals without barrel nets, which would reveal their roles in the functioning of the cerebral cortex. Barrel nets seem to be useful for addressing important questions about intracortical local circuits.

Funding

This work was supported by Grant-in-Aid for Scientific Research from the Ministry of Education, Culture, Sports, Science and Technology-Japan (25290013, 25640032, 25123702, 26111708); Takeda Science Foundation; Takeda Medical Research Foundation; Astellas Foundation for Research on Metabolic Disorders; the Kurata Memorial Hitachi Science and Technology Foundation; Mitsubishi Foundation; and Research Foundation for Opto-Science and Technology. This work was also supported by a Research Fellowship for Young Scientists from Japan Society for the Promotion of Science (to K.S.).

Notes

We thank Drs. M. Takeichi (RIKEN CDB) and J. Frisén (Karolinska Institutet) for plasmids. We are grateful to Drs. S. Tsuji, T. Kadowaki, H. Bito (The University of Tokyo), E. Nishida (Kyoto University), Y. Sasai (RIKEN CDB) and S. Nakanishi (Osaka Bioscience Institute) for their continuous support and warm encouragement. We express our gratitude to Drs. T. Sakurai and M. Sato (Kanazawa University) for their technical support. We thank Kawasaki lab members and Z. Blalock for critical discussions and comments on this manuscript, and K. Tanno for technical assistance. *Conflict of Interest*: None declared.

References

Ako R, Wakimoto M, Ebisu H, Tanno K, Hira R, Kasai H, Matsuzaki M, Kawasaki H. 2011. Simultaneous visualization of multiple neuronal properties with single-cell resolution in the living rodent brain. Mol Cell Neurosci. 48:246-257.

Arlotta P, Molyneaux BJ, Chen J, Inoue J, Kominami R, Macklis JD. 2005. Neuronal subtype-specific genes that control corticospinal motor neuron development in vivo. Neuron. 45:207-221.

Barnabé-Heider F, Meletis K, Eriksson M, Bergmann O, Sabelström H, Harvey MA, Mikkers H, Frisén J. 2008. Genetic manipulation of adult mouse neurogenic niches by in vivo electroporation. Nat Methods. 5:189-196.

Bozdagi O, Valcin M, Poskanzer K, Tanaka H, Benson DL. 2004. Temporally distinct demands for classic cadherins in synapse formation and maturation. Mol Cell Neurosci. 27:509-521.

Dye CA, El Shawa H, Huffman KJ. 2011. A lifespan analysis of intraneocortical connections and gene expression in the mouse II. Cereb Cortex. 21:1331-1350.

Erzurumlu RS, Gaspar P. 2012. Development and critical period plasticity of the barrel cortex. Eur J Neurosci. 35:1540-1553.

Erzurumlu RS, Kind PC. 2001. Neural activity: sculptor of 'barrels' in the neocortex. Trends Neurosci. 24:589-595.

Fox K. 2008. Development of barrel cortex + Experience-dependent plasticity. In: Fox K, editor. Barrel Cortex. Cambridge: Cambridge University Press. p. 79-216.

Fremeau RT, Jr., Troyer MD, Pahner I, Nygaard GO, Tran CH, Reimer RJ, Bellocchio EE, Fortin D, Storm-Mathisen J, Edwards RH. 2001. The expression of vesicular

glutamate transporters defines two classes of excitatory synapse. Neuron. 31:247-260.

Fujimori T, Takeichi M. 1993. Disruption of epithelial cell-cell adhesion by exogenous expression of a mutated nonfunctional N-cadherin. Mol Biol Cell. 4:37-47.

Fujiyama F, Furuta T, Kaneko T. 2001. Immunocytochemical localization of candidates for vesicular glutamate transporters in the rat cerebral cortex. J Comp Neurol. 435:379-387.

Gil OD, Needleman L, Huntley GW. 2002. Developmental patterns of cadherin expression and localization in relation to compartmentalized thalamocortical terminations in rat barrel cortex. J Comp Neurol. 453:372-388.

Hayakawa I, Kawasaki H. 2010. Rearrangement of retinogeniculate projection patterns after eye-specific segregation in mice. PLoS One. 5:e11001.

Hertel N, Redies C. 2011. Absence of layer-specific cadherin expression profiles in the neocortex of the reeler mutant mouse. Cereb Cortex. 21:1105-1117.

Hevner RF, Daza RA, Rubenstein JL, Stunnenberg H, Olavarria JF, Englund C. 2003. Beyond laminar fate: toward a molecular classification of cortical projection/pyramidal neurons. Dev Neurosci. 25:139-151.

Huntley GW. 2002. Dynamic aspects of cadherin-mediated adhesion in synapse development and plasticity. Biol Cell. 94:335-344.

Huntley GW, Benson DL. 1999. Neural (N)-cadherin at developing thalamocortical synapses provides an adhesion mechanism for the formation of somatopically organized connections. J Comp Neurol. 407:453-471.

Inoue T, Tanaka T, Suzuki SC, Takeichi M. 1998. Cadherin-6 in the developing mouse brain:

expression along restricted connection systems and synaptic localization suggest a potential role in neuronal circuitry. Dev Dyn. 211:338-351.

Inoue YU, Asami J, Inoue T. 2008. Cadherin-6 gene regulatory patterns in the postnatal mouse brain. Mol Cell Neurosci. 39:95-104.

Iwai L, Kawasaki H. 2009. Molecular development of the lateral geniculate nucleus in the absence of retinal waves during the time of retinal axon eye-specific segregation. Neuroscience. 159:1326-1337.

Iwai L, Ohashi Y, van der List D, Usrey WM, Miyashita Y, Kawasaki H. 2013. FoxP2 is a parvocellular-specific transcription factor in the visual thalamus of monkeys and ferrets. Cereb Cortex. 23:2204-2212.

Kawasaki H, Crowley JC, Livesey FJ, Katz LC. 2004. Molecular organization of the ferret visual thalamus. J Neurosci. 24:9962-9970.

Kawasaki H, Iwai L, Tanno K. 2012. Rapid and efficient genetic manipulation of gyrencephalic carnivores using in utero electroporation. Mol Brain. 5:24.

Kawasaki H, Toda T, Tanno K. 2013. In vivo genetic manipulation of cortical progenitors in gyrencephalic carnivores using in utero electroporation. Biol Open. 2:95-100.

Kawauchi T, Sekine K, Shikanai M, Chihama K, Tomita K, Kubo K, Nakajima K, Nabeshima Y, Hoshino M. 2010. Rab GTPases-dependent endocytic pathways regulate neuronal migration and maturation through N-cadherin trafficking. Neuron. 67:588-602.

Krishna-K K, Hertel N, Redies C. 2011. Cadherin expression in the somatosensory cortex: evidence for a combinatorial molecular code at the single-cell level. Neuroscience. 175:37-48.

Lefkovics K, Mayer M, Bercsényi K, Szabó G, Lele Z. 2012. Comparative analysis of type II classic cadherin mRNA distribution patterns in the developing and adult mouse somatosensory cortex and hippocampus suggests significant functional redundancy. J Comp Neurol. 520:1387-1405.

López-Bendito G, Molnár Z. 2003. Thalamocortical development: how are we going to get there? Nat Rev Neurosci. 4:276-289.

Matsuda T, Cepko CL. 2007. Controlled expression of transgenes introduced by in vivo electroporation. Proc Natl Acad Sci U S A. 104:1027-1032.

Meijering E. 2010. Neuron tracing in perspective. Cytometry A. 77:693-704.

Meijering E, Jacob M, Sarria JC, Steiner P, Hirling H, Unser M. 2004. Design and validation of a tool for neurite tracing and analysis in fluorescence microscopy images. Cytometry A. 58:167-176.

Meyer HS, Wimmer VC, Hemberger M, Bruno RM, de Kock CP, Frick A, Sakmann B, Helmstaedter M. 2010a. Cell type-specific thalamic innervation in a column of rat vibrissal cortex. Cereb Cortex. 20:2287-2303.

Meyer HS, Wimmer VC, Oberlaender M, de Kock CP, Sakmann B, Helmstaedter M. 2010b. Number and laminar distribution of neurons in a thalamocortical projection column of rat vibrissal cortex. Cereb Cortex. 20:2277-2286.

Nakagawa Y, O'Leary DD. 2003. Dynamic patterned expression of orphan nuclear receptor genes RORalpha and RORbeta in developing mouse forebrain. Dev Neurosci. 25:234-244.

Nieman MT, Kim JB, Johnson KR, Wheelock MJ. 1999. Mechanism of extracellular domain-deleted dominant negative cadherins. J Cell Sci. 112 (Pt 10):1621-1632.

Niwa H, Yamamura K, Miyazaki J. 1991. Efficient selection for high-expression transfectants with a novel eukaryotic vector. Gene. 108:193-199.

O'Leary DD, Ruff NL, Dyck RH. 1994. Development, critical period plasticity, and adult reorganizations of mammalian somatosensory systems. Curr Opin Neurobiol. 4:535-544.

Oberlaender M, de Kock CP, Bruno RM, Ramirez A, Meyer HS, Dercksen VJ, Helmstaedter M, Sakmann B. 2012. Cell type-specific three-dimensional structure of thalamocortical circuits in a column of rat vibrissal cortex. Cereb Cortex. 22:2375-2391.

Obst-Pernberg K, Medina L, Redies C. 2001. Expression of R-cadherin and N-cadherin by cell groups and fiber tracts in the developing mouse forebrain: relation to the formation of functional circuits. Neuroscience. 106:505-533.

Osterhout JA, Josten N, Yamada J, Pan F, Wu SW, Nguyen PL, Panagiotakos G, Inoue YU, Egusa SF, Volgyi B, Inoue T, Bloomfield SA, Barres BA, Berson DM, Feldheim DA, Huberman AD. 2011. Cadherin-6 mediates axon-target matching in a non-image-forming visual circuit. Neuron. 71:632-639.

R Core Team. 2014. R: A language and environment for statistical computing. Version 3.1.0. Vienna, Austria: R Foundation for Statistical Computing. URL http://R-project.org/.

Rebsam A, Gaspar P. 2006. Presynaptic mechanisms controlling axon terminals remodeling in the thalamocortical and retinogeniculate systems. In: Erzurumlu RS, Guido W, Molnar Z, editors. Development and Plasticity in Sensory Thalamus and Cortex. New York: Springer. p. 183-207.

Redies C, Takeichi M. 1996. Cadherins in the developing central nervous system: an adhesive code for segmental and functional subdivisions. Dev Biol. 180:413-423.

Riehl R, Johnson K, Bradley R, Grunwald GB, Cornel E, Lilienbaum A, Holt CE. 1996. Cadherin function is required for axon outgrowth in retinal ganglion cells in vivo. Neuron. 17:837-848.

Schaeren-Wiemers N, André E, Kapfhammer JP, Becker-André M. 1997. The expression pattern of the orphan nuclear receptor RORbeta in the developing and adult rat nervous system suggests a role in the processing of sensory information and in circadian rhythm. Eur J Neurosci. 9:2687-2701.

Sehara K, Kawasaki H. 2011. Neuronal circuits with whisker-related patterns. Mol Neurobiol. 43:155-162.

Sehara K, Toda T, Iwai L, Wakimoto M, Tanno K, Matsubayashi Y, Kawasaki H. 2010. Whisker-related axonal patterns and plasticity of layer 2/3 neurons in the mouse barrel cortex. J Neurosci. 30:3082-3092.

Sehara K, Wakimoto M, Ako R, Kawasaki H. 2012. Distinct developmental principles underlie the formation of ipsilateral and contralateral whisker-related axonal patterns of layer 2/3 neurons in the barrel cortex. Neuroscience. 226:289-304.

Suzuki SC, Inoue T, Kimura Y, Tanaka T, Takeichi M. 1997. Neuronal circuits are subdivided by differential expression of type-II classic cadherins in postnatal mouse brains. Mol Cell Neurosci. 9:433-447.

Takeichi M. 1991. Cadherin cell adhesion receptors as a morphogenetic regulator. Science. 251:1451-1455.

Takeichi M. 2007. The cadherin superfamily in neuronal connections and interactions. Nat Rev Neurosci. 8:11-20.

Tepass U, Truong K, Godt D, Ikura M, Peifer M. 2000. Cadherins in embryonic and neural

morphogenesis. Nat Rev Mol Cell Biol. 1:91-100.

Terakawa YW, Inoue YU, Asami J, Hoshino M, Inoue T. 2013. A sharp cadherin-6 gene expression boundary in the developing mouse cortical plate demarcates the future functional areal border. Cereb Cortex. 23:2293-2308.

Toda T, Hayakawa I, Matsubayashi Y, Tanaka K, Ikenaka K, Lu QR, Kawasaki H. 2008. Termination of lesion-induced plasticity in the mouse barrel cortex in the absence of oligodendrocytes. Mol Cell Neurosci. 39:40-49.

Toda T, Homma D, Tokuoka H, Hayakawa I, Sugimoto Y, Ichinose H, Kawasaki H. 2013. Birth regulates the initiation of sensory map formation through serotonin signaling. Dev Cell. 27:32-46.

Togashi H, Abe K, Mizoguchi A, Takaoka K, Chisaka O, Takeichi M. 2002. Cadherin regulates dendritic spine morphogenesis. Neuron. 35:77-89.

Williams ME, Wilke SA, Daggett A, Davis E, Otto S, Ravi D, Ripley B, Bushong EA, Ellisman MH, Klein G, Ghosh A. 2011. Cadherin-9 regulates synapse-specific differentiation in the developing hippocampus. Neuron. 71:640-655.

Woolsey TA. 1990. Peripheral alteration and somatosensory development. In: Coleman JR, editor. Development of Sensory Systems in Mammals. New York: Wiley. p. 461-516.

Yamasaki T, Kawasaki H, Arakawa S, Shimizu K, Shimizu S, Reiner O, Okano H, Nishina S, Azuma N, Penninger JM, Katada T, Nishina H. 2011. Stress-activated protein kinase MKK7 regulates axon elongation in the developing cerebral cortex. J Neurosci. 31:16872-16883.

Figure Legends

Figure 1. The effect of dn-cadherin on migration of transfected layer 2/3 neurons

(*A*) Layer 2/3 neurons were transfected with pCAG-GFP plus either pCAG vector (control) or pCAG-hDNcad (hDNcad) using *in utero* electroporation at E15.5. Coronal sections were prepared at P16 and stained with Hoechst 33342. Note that migration of GFP-positive transfected layer 2/3 neurons was severely impaired by hDNcad expression (arrowheads). Cortical layers are indicated with numbers. Scale bar = 150 μm. (*B*) Experimental procedure for temporal regulation of dn-cadherin expression. After layer 2/3 neurons were transfected with the indicated plasmids using *in utero* electroporation, pups were treated with 4-OHT at the indicated time points during development. Coronal sections were prepared 5 days later and stained with Hoechst 33342. (*C*) Migration was impaired by 4-OHT treatment at P0 (arrowheads), but not by the treatment at P2 or P4 in hDNcad sample. The experiments were performed as described in (*B*). Cortical layers are indicated with numbers. Scale bar = 250 μm.

Figure 2. Efficient gene expression was achieved by multiple 4-OHT treatments

(*A*) Experimental procedure. After layer 2/3 neurons were co-transfected with *in utero* electroporation at E15.5, pups were treated with 4-OHT once or 3 times daily. Coronal sections were prepared at P10 and stained with Hoechst 33342. (*B*) 4-OHT treatment for 3 consecutive days gave higher recombination efficiency. Note that transfection efficiency was indistinguishable between 1-day and 3-day treatment as revealed with mCherry signals, whereas GFP signals were markedly enhanced by 3-day treatment. Cortical layers are indicated with numbers. Scale bar = 100 μm.

Figure 3. The effects of dn-cadherin expression on barrel net patterns in tangential sections

(*A*) Experimental procedure. After layer 2/3 neurons were transfected with the indicated plasmids using *in utero* electroporation at E15.5, pups were treated with 4-OHT 3 times at the indicated time points. Tangential sections were prepared at P15, and sections containing layer 4 were stained with Hoechst 33342. (*B*) Expression of hDNcad in layer 2/3 neurons strongly inhibited barrel net formation (hDNcad), while control plasmid did not affect barrel net patterns (control). (*C*) Expression of cN390Δ, another dn-cadherin construct, gave consistent results. Note that the pattern of cytoarchitectonic barrels revealed with Hoechst staining was not apparently affected by dn-cadherin expression (lower panels). Scale bars = 200 μm.

Figure 4. The effects of dn-cadherin expression on barrel net patterns in coronal sections

(*A*) *In utero* electroporation and 4-OHT treatment were performed as described in Figure 3*A*. Coronal sections were prepared at P15 and stained with anti-VGLUT2 antibody, which visualizes whisker-related patterns of thalamocortical axon (TCA) patches. Confocal microscopic images are shown. Although GFP-positive axons are predominantly accumulated in septal regions of control samples (arrows), such accumulation was severely impaired in dn-cadherin samples (hDNcad and cN390Δ). Note that TCA patches revealed with VGLUT2 antibody were not apparently affected by dn-cadherin. Arrowheads indicate septal regions revealed with VGLUT2 staining. Cortical layers are indicated with numbers. Scale bar = 50 μm. (*B*) Quantitative analyses of the effects of dn-cadherin on barrel net formation (see Supplementary Figure 3 and Materials and Methods for detailed procedures). The p/c ratio of GFP signals was significantly lower in hDNcad samples, while the c/p ratio of VGLUT2 was

not. *$p < 0.05$, N.S. $p > 0.3$, Welch's *t*-test. Error bars indicate the standard error of the mean (SEM). n = 3 pups for control, 3 pups for hDNcad. (*C*) High magnification confocal microscopic analysis of GFP-positive axons in septal regions and barrel hollows. GFP-positive fine axons in septal regions were much fewer in hDNcad samples than in control samples. Scale bar = 20 μm. (*D*) Quantitative analysis of the numbers of GFP-positive neurons in layer 2/3. Coronal sections of 50 μm thickness were examined using a confocal microscope, and the densities of GFP-positive cells were examined. No significant difference was detected between control and hDNcad samples (N.S. $p > 0.5$, Mann-Whitney's *U*-test; n = 3 pups for control, 3 pups for hDNcad). Error bars indicate SEM.

Figure 5. The effect of dn-cadherin expression on callosal axons derived from layer 2/3 neurons

In utero electroporation and 4-OHT treatment were performed as described in Figure 3*A*. Coronal sections were prepared at P15, and were stained with Hoechst 33342. The cortex contralateral to the transfected side is shown, and therefore GFP-positive axons are callosal axons derived from layer 2/3 neurons of transfected side (not shown). The extension of GFP-positive callosal axons was not suppressed by hDNcad expression (arrowheads). Scale bar = 1 mm.

Figure 6. The effects of dn-cadherin on the morphology of layer 2/3 neurons *in vitro*

(*A*) Representative images of primary cultured layer 2/3 neurons electroporated with GFP expression plasmids plus either control (left) or hDNcad expression (right) plasmids at E15.5. Note that their morphologies were indistinguishable from each other. Scale bar = 100 μm. (*B-E*) Quantification of morphologies of the transfected neurons. No significant differences

were observed in the number of branches (*B*), total axon length (*C*), the length of the primary axon branch (*D*) and the length of higher-order axon branches (*E*). N.S. $p > 0.1$, Welch's *t*-test; n = 7 for each sample. Error bars in all graphs indicate SEM.

Figure 7. The expression patterns of layer markers in the hDNcad-transfected cortex

In utero electroporation and 4-OHT treatment were performed as described in Figure 3*A*. Coronal sections were stained with anti-Brn2, anti-RORβ and anti-Ctip2 antibodies. (*A*, *B*) Confocal microscopic images of Brn2 and Ctip2 at P15 (*A*) and of RORβ at P5 (*B*). The expression of layer markers was not affected in GFP-positive hDNcad-transfected neurons. Cortical layers are indicated with numbers. Scale bars = 150 μm. (*C*) Quantification of marker expression. The numbers of GFP-positive cells examined are indicated in parenthesis. (*D*, *E*) High-magnification confocal microscopic images at P15 (*D*) and P5 (*E*). Brn2, Ctip2 and RORβ signals were localized in Hoechst-positive nuclei. Scale bars = 20 μm.

Figure 8. The effect of hDNcad on presynaptic structures on barrel nets

(*A*) Developmental time course of the formation of presynaptic structures. Layer 2/3 neurons were transfected with pCAG-mCherry and pCAG-synaptophysin-GFP at E15.5, and coronal sections were prepared at the indicated ages. Septal regions in layer 4 are shown. mCherry-positive axons of layer 2/3 neurons in barrel nets increased from P5 to P15. Accordingly, GFP-positive puncta also markedly increased (arrowheads). Scale bar = 25 μm. (*B*) The effect of hDNcad on presynaptic structures on barrel nets. Layer 2/3 neurons were transfected with pCAG-synaptophysin-mCherry, pCAG-ER^{T2}CreER^{T2}, pCAG-floxedSTOP-GFP plus either pCAG-floxedSTOP-hDNcad or pCAG-floxedSTOP control vector at E15.5, and pups were treated with 4-OHT 3 times. Coronal sections were

prepared at P15. Septal regions in layer 4 are shown. The expression of hDNcad resulted in the reduction of mCherry-positive puncta (arrowheads). Scale bar = 25 µm. (*C*) High magnification images of mCherry-positive puncta (red, arrowheads) and GFP-positive axon branches (green). Scale bar = 1 µm. (*D*) The density of mCherry-positive puncta along GFP-positive axons in hDNcad samples was not significantly different from that in control samples. N.S. $p > 0.2$, Mann-Whitney's *U*-test; n = 3 pups for both conditions. Error bars indicate SEM. (*E*) The size of individual mCherry-positive puncta in hDNcad samples was not significantly different from that in control samples. N.S. $p > 0.2$, Mann-Whitney's *U*-test; n = 3 pups for both conditions. Error bars indicate SEM.

Figure 9. Cadherin is required for the formation, rather than the maintenance, of barrel nets

(*A*) Experimental procedure for examining time course of barrel net formation. *In utero* electroporation and 4-OHT treatment were performed as described, and coronal sections were prepared at the indicated time points. (*B*) Barrel nets were not visible at any ages examined in hDNcad samples, while the pattern of barrel nets was visible after P10 in control samples (arrows). Arrowheads indicate septal regions. Scale bar = 250 µm. (*C*) Experimental procedures for early and late 4-OHT treatments. *In utero* electroporation was performed as described in Figure 9*A*, and 4-OHT treatment was performed at P2-P4 (early 4-OHT) or P15-P17 (late 4-OHT). Coronal sections were prepared about two weeks later, and stained with Hoechct 33342. (*D*) The effects of early and late 4-OHT treatments on barrel net patterns. Note that barrel net patterns were strongly disrupted by early 4-OHT treatment, while they were not affected by late 4-OHT treatment (arrows). Arrowheads indicate the septal region. Scale bar = 200 µm. (*E*) Quantification of the p/c ratio. Early 4-OHT treatment significantly

reduced the p/c ratio in hDNcad-transfected samples, while late 4-OHT treatment did not. *$p < 0.05$, N.S. $p > 0.2$, Welch's *t*-test (early 4-OHT, control, n = 3 pups; early 4-OHT, hDNcad, n = 3 pups; late 4-OHT, control, n = 4 pups; late 4-OHT, hDNcad, n = 3 pups). Error bars indicate SEM.

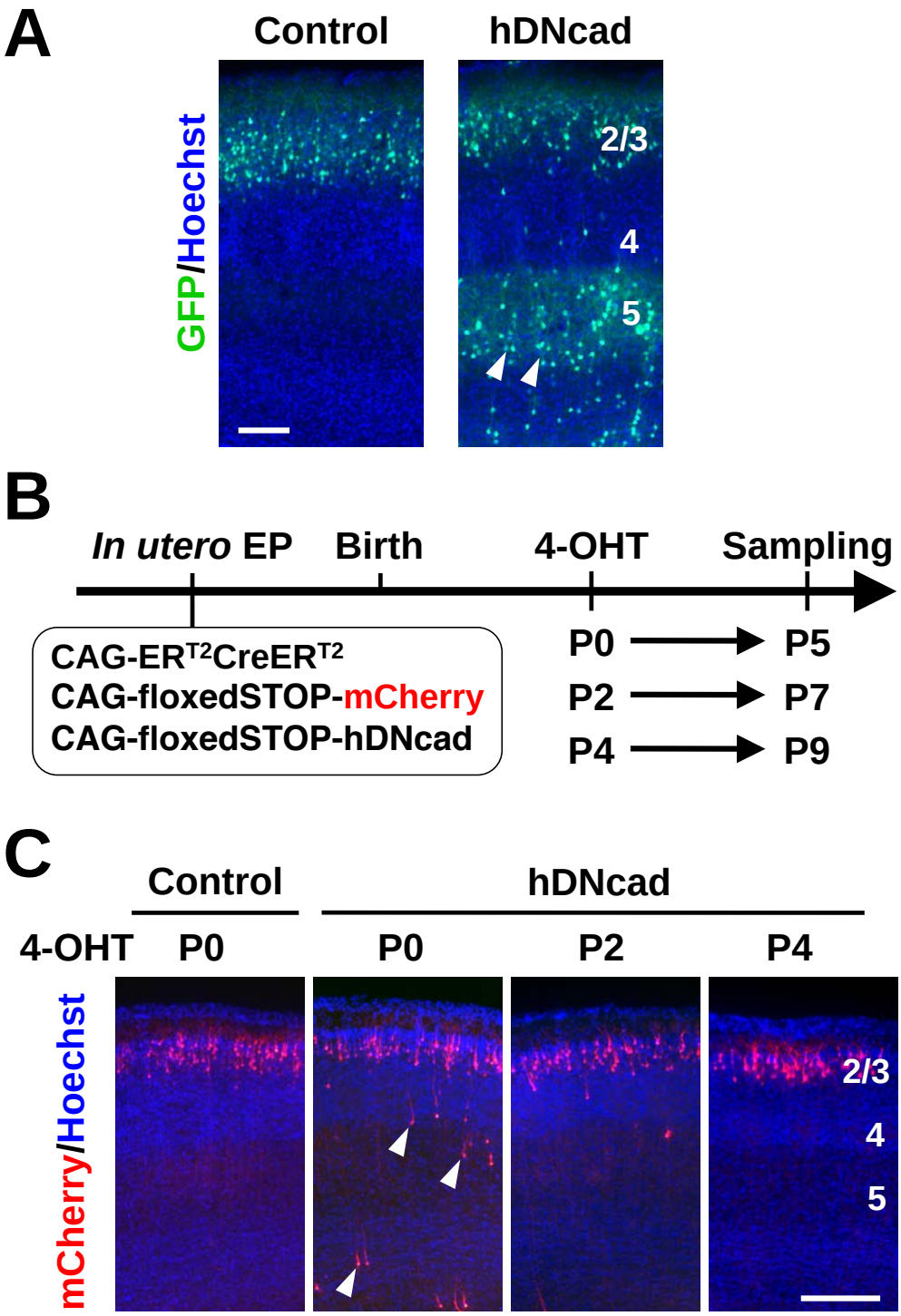
A
Control
hDNcad
GFP/Hoechst
2/3
4
5
B
In utero EP
Birth
4-OHT
Sampling
CAG-ERT2CreERT2
CAG-floxedSTOP-mCherry
CAG-floxedSTOP-hDNcad
P0
P5
P2
P7
P4
P9
C
Control
hDNcad
4-OHT
P0
P0
P2
P4
mCherry/Hoechst
2/3
4
5

Figure 1

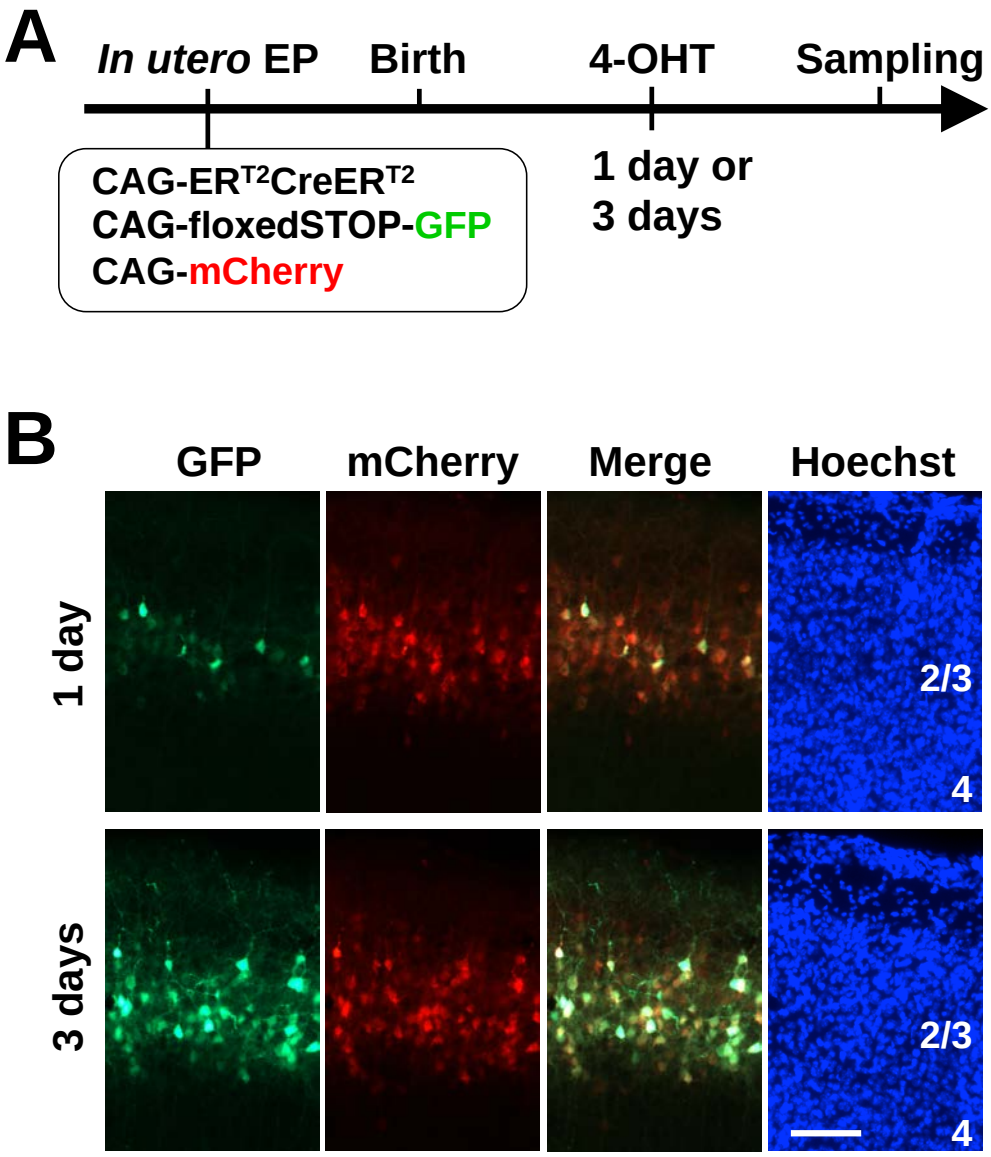
A
In utero EP
Birth
4-OHT
Sampling
CAG-ERT2CreERT2
CAG-floxedSTOP-GFP
CAG-mCherry
1 day or
3 days
B
GFP
mCherry
Merge
Hoechst
1 day
3 days
2/3
4
2/3
4

Figure 2

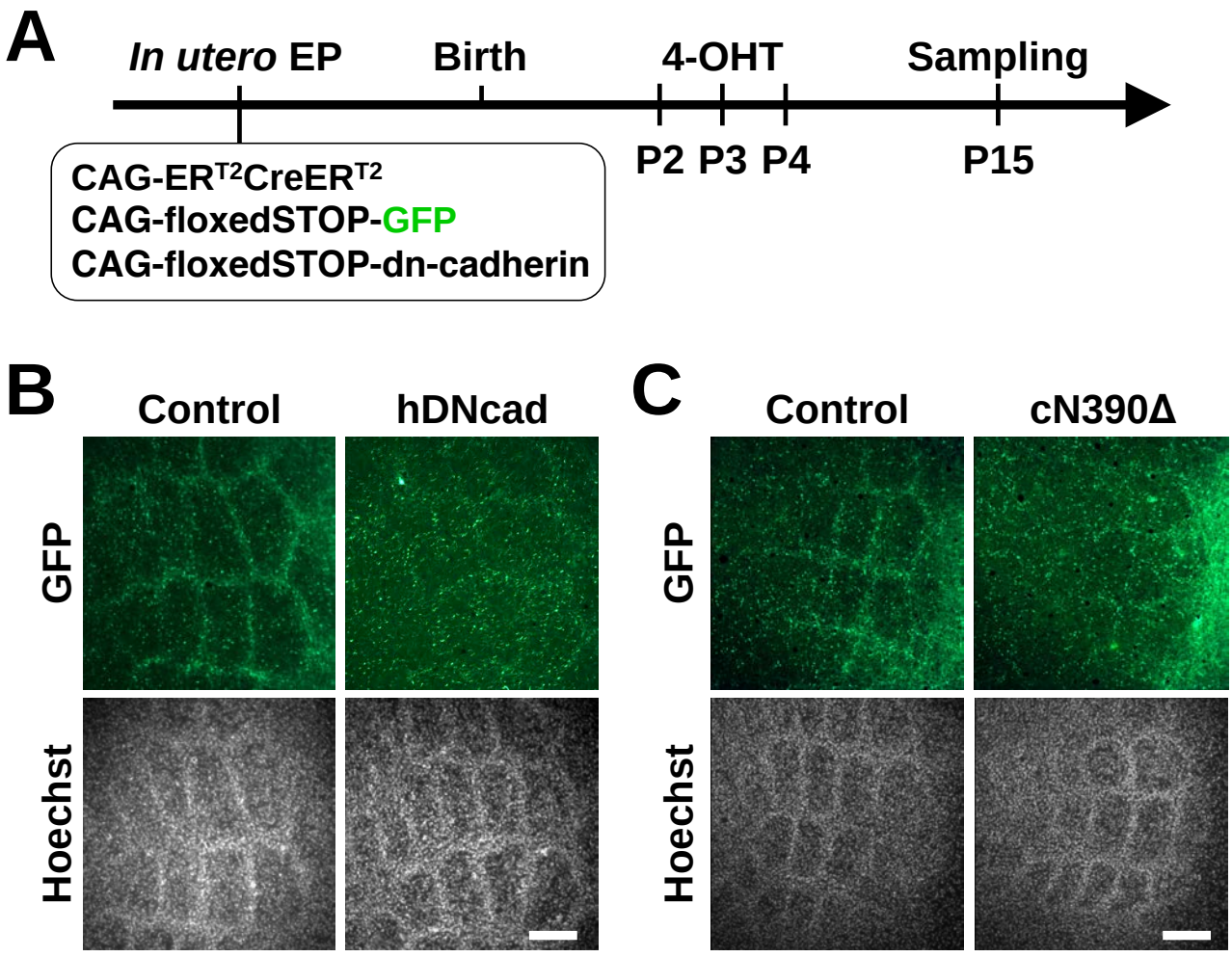
A
In utero EP
Birth
4-OHT
Sampling
P2 P3 P4
P15
CAG-ERT2CreERT2
CAG-floxedSTOP-GFP
CAG-floxedSTOP-dn-cadherin
B
Control
hDNcad
GFP
Hoechst
C
Control
cN390Δ
GFP
Hoechst

Figure 3

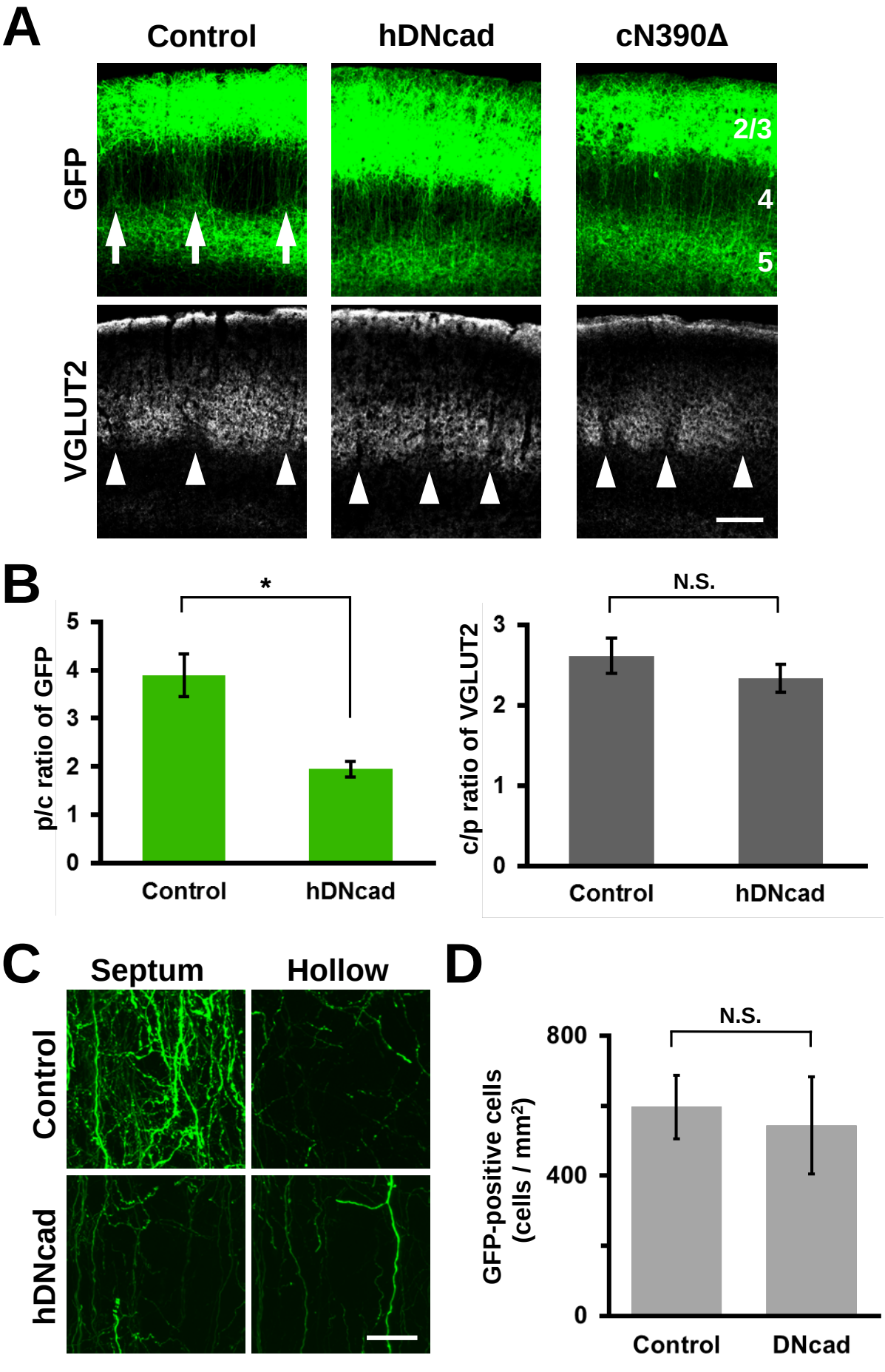
A
Control
hDNcad
cN390Δ
GFP
VGLUT2
2/3
4
5
B
*
N.S.
p/c ratio of GFP
c/p ratio of VGLUT2
Control
hDNcad
C
Septum
Hollow
Control
hDNcad
D
N.S.
GFP-positive cells (cells / mm²)
800
400
0
Control
DNcad

Figure 4

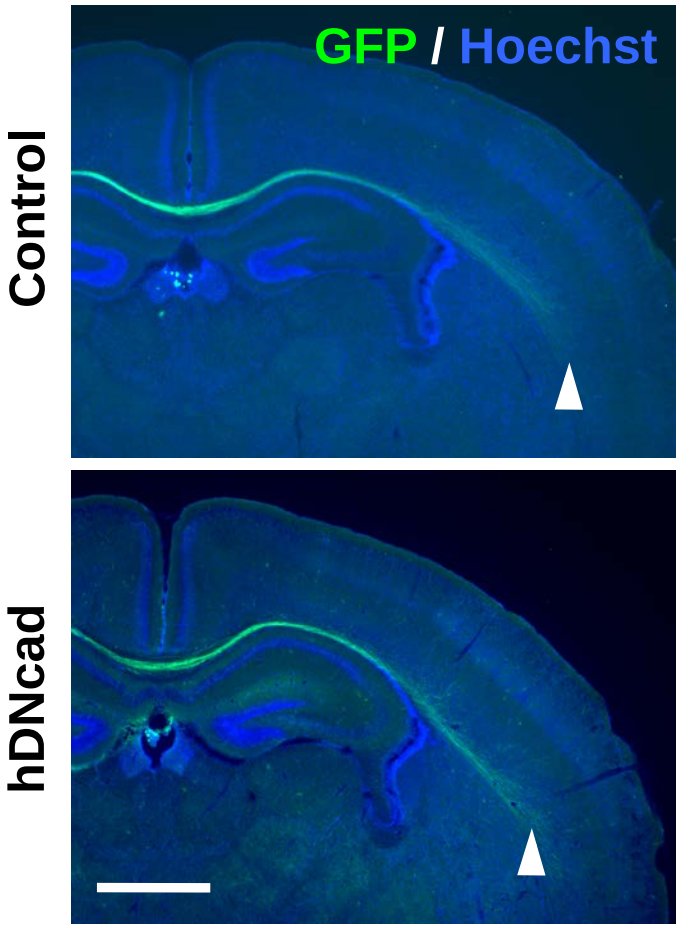

Figure 5

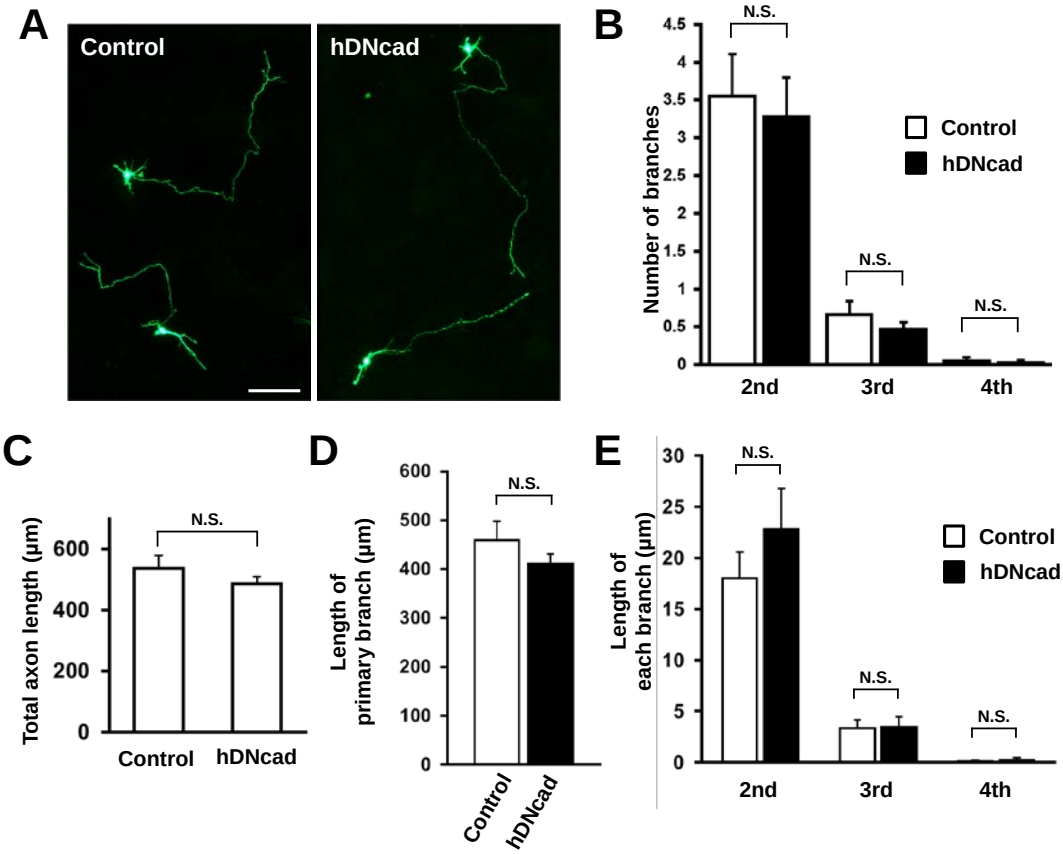
A
Control
hDNcad
B
N.S.
Number of branches
Control
hDNcad
2nd
3rd
4th
C
Total axon length (μm)
Control
hDNcad
D
Length of primary branch (μm)
E
Length of each branch (μm)

Figure 6

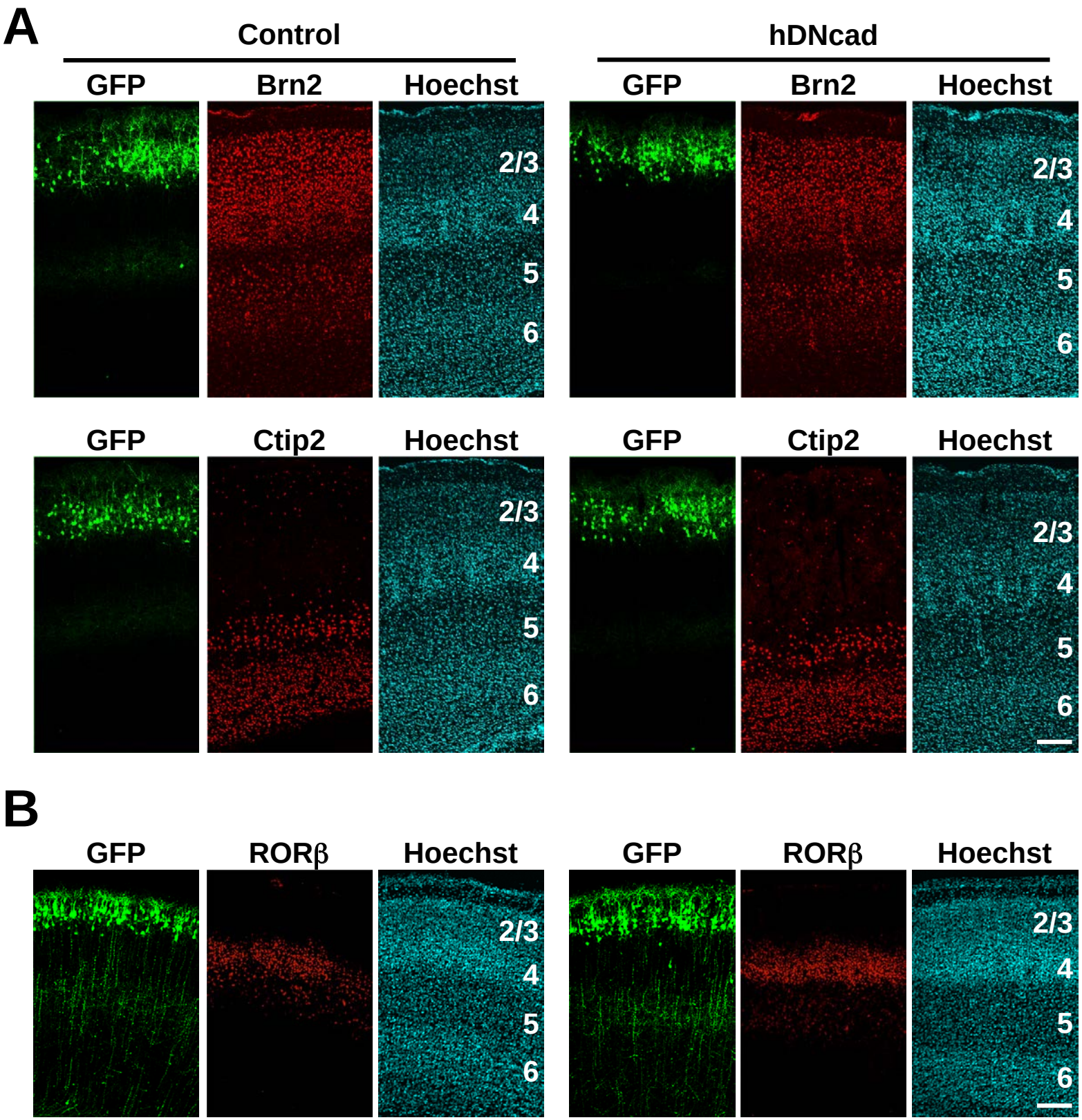
A
Control
hDNcad
GFP
Brn2
Hoechst
GFP
Brn2
Hoechst
2/3
4
5
6
2/3
4
5
6
GFP
Ctip2
Hoechst
GFP
Ctip2
Hoechst
2/3
4
5
6
2/3
4
5
6
B
GFP
RORβ
Hoechst
GFP
RORβ
Hoechst
2/3
4
5
6
2/3
4
5
6

Figure 7AB

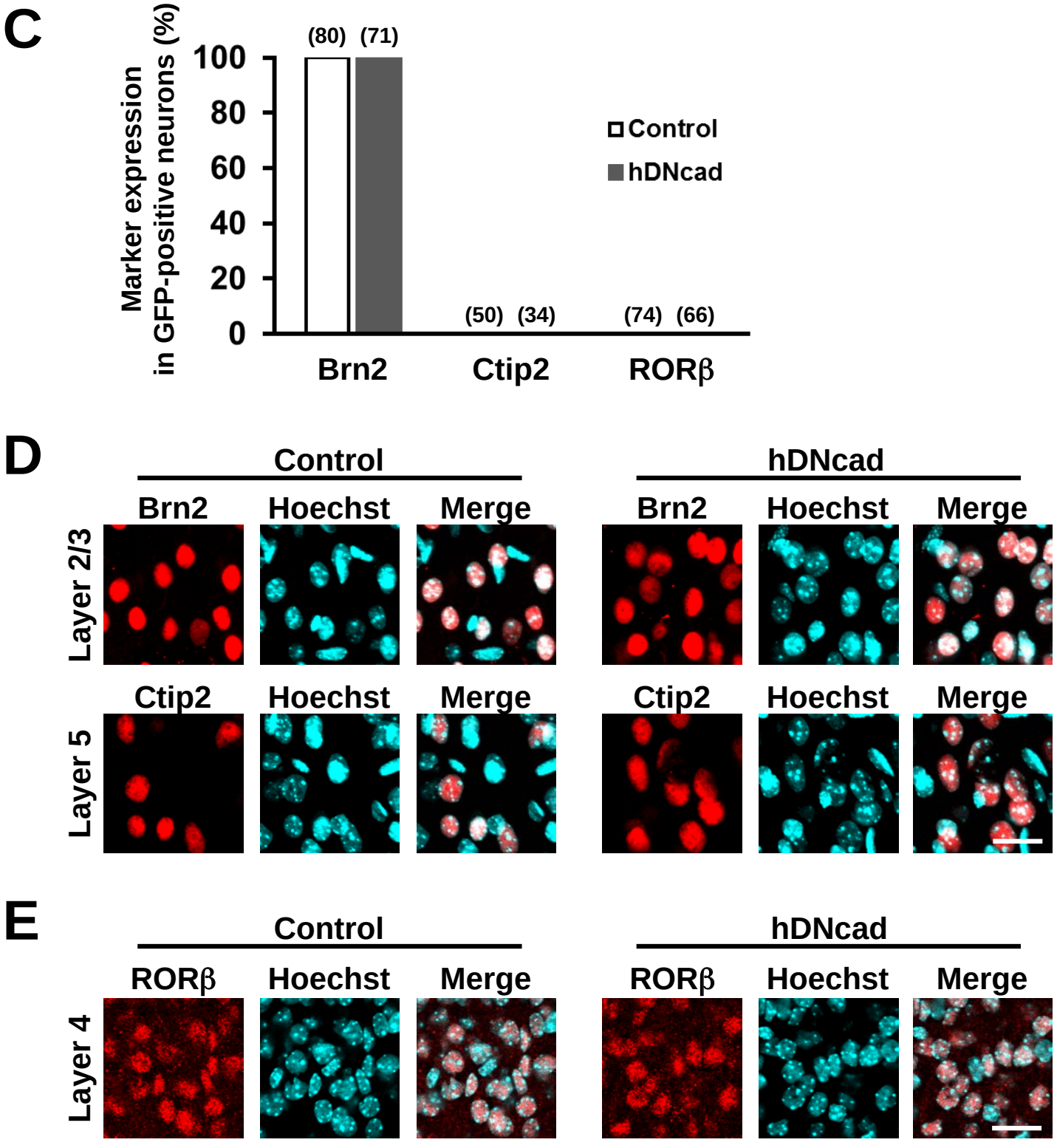
C
Marker expression in GFP-positive neurons (%)
100
80
60
40
20
0
(80) (71)
(50) (34)
(74) (66)
Control
hDNcad
Brn2
Ctip2
RORβ
D
Control
hDNcad
Brn2
Hoechst
Merge
Layer 2/3
Ctip2
Layer 5
E
RORβ

Figure 7CDE

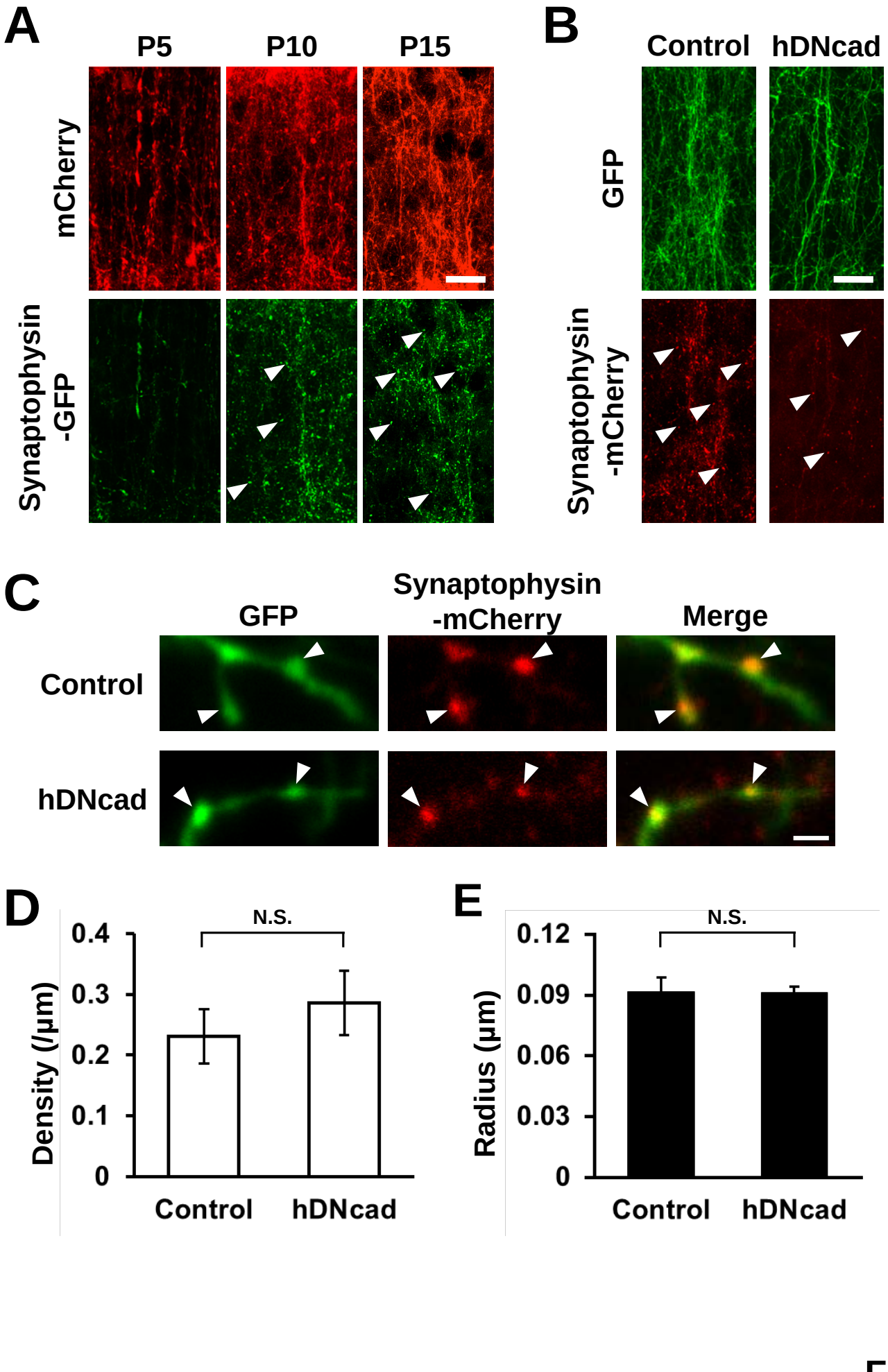
A
P5
P10
P15
mCherry
Synaptophysin
-GFP
B
Control
hDNcad
GFP
Synaptophysin
-mCherry
C
GFP
Synaptophysin
-mCherry
Merge
Control
hDNcad
D
N.S.
0.4
0.3
0.2
0.1
0
Density (/μm)
Control
hDNcad
E
N.S.
0.12
0.09
0.06
0.03
0
Radius (μm)
Control
hDNcad

Figure 8

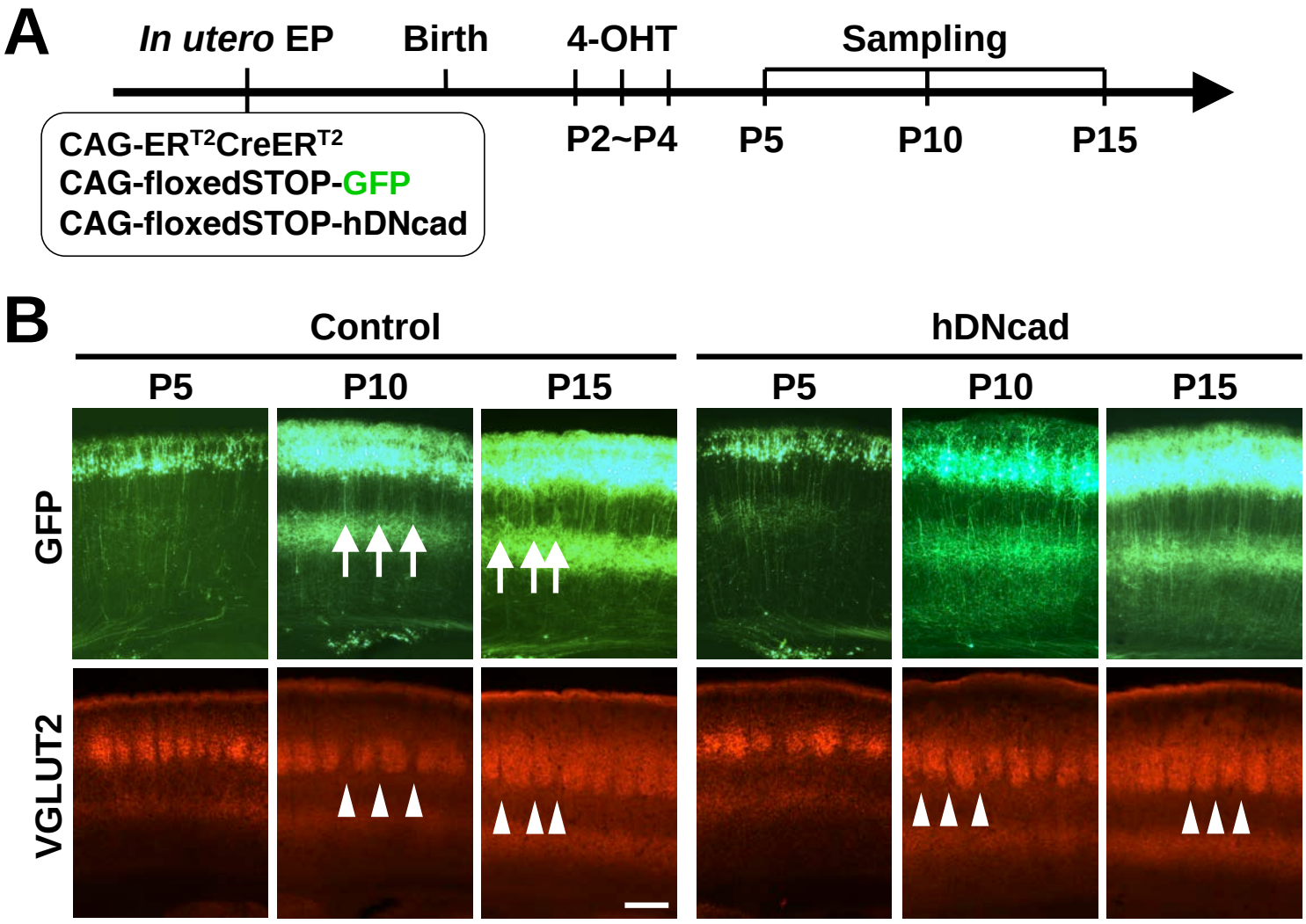
A
In utero EP
Birth
4-OHT
Sampling
P2~P4
P5
P10
P15
CAG-ERT2CreERT2
CAG-floxedSTOP-GFP
CAG-floxedSTOP-hDNcad
B
Control
hDNcad
P5
P10
P15
P5
P10
P15
GFP
VGLUT2

Figure 9AB

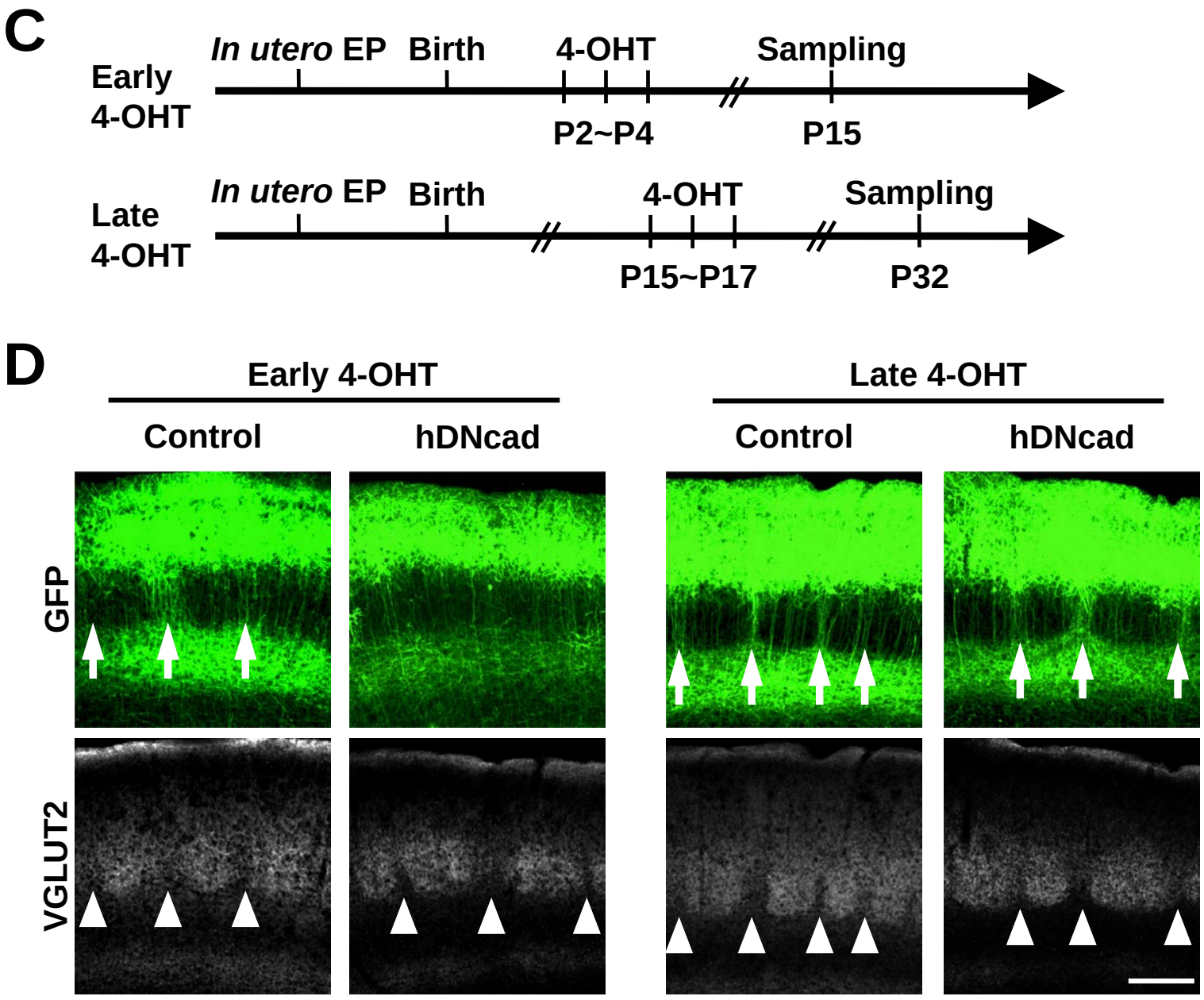
C
Early 4-OHT
In utero EP
Birth
4-OHT
Sampling
P2~P4
P15
Late 4-OHT
In utero EP
Birth
4-OHT
Sampling
P15~P17
P32
D
Early 4-OHT
Late 4-OHT
Control
hDNcad
Control
hDNcad
GFP
VGLUT2
E
p/c ratio of GFP
5
3
1
*
N.S.
Early 4-OHT
Late 4-OHT
Control
hDNcad

Figure 9CDE

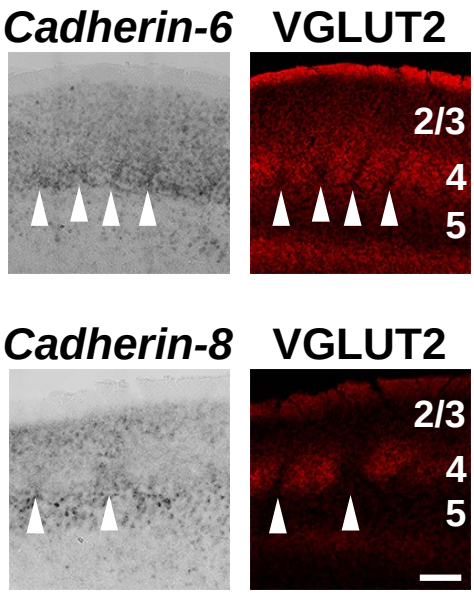

Supplementary Figure 1

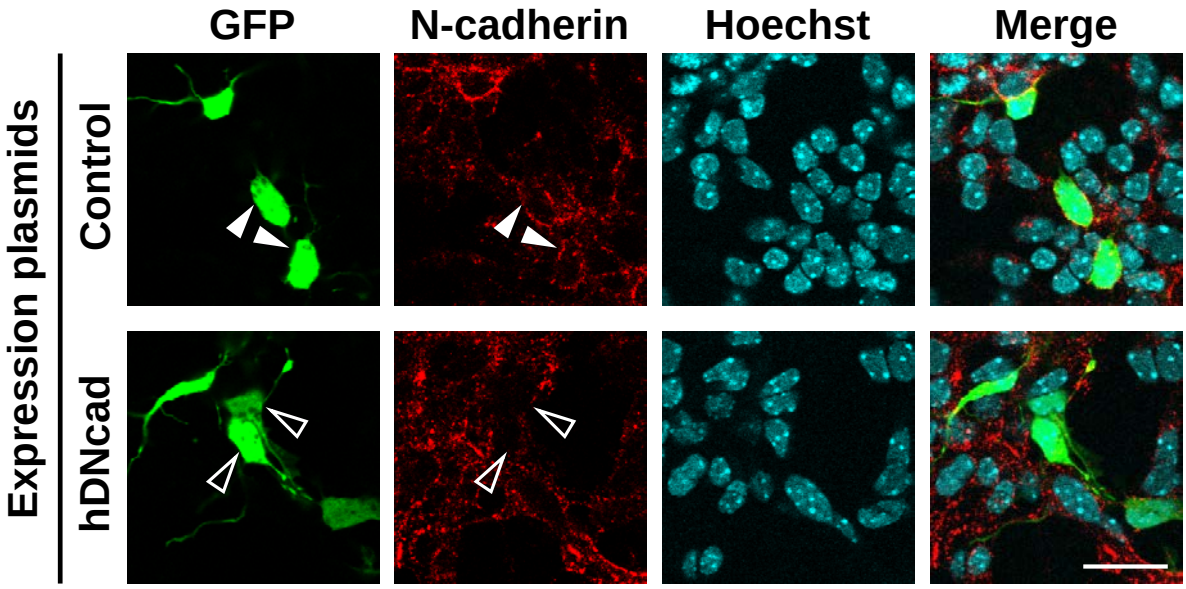

Supplementary Figure2

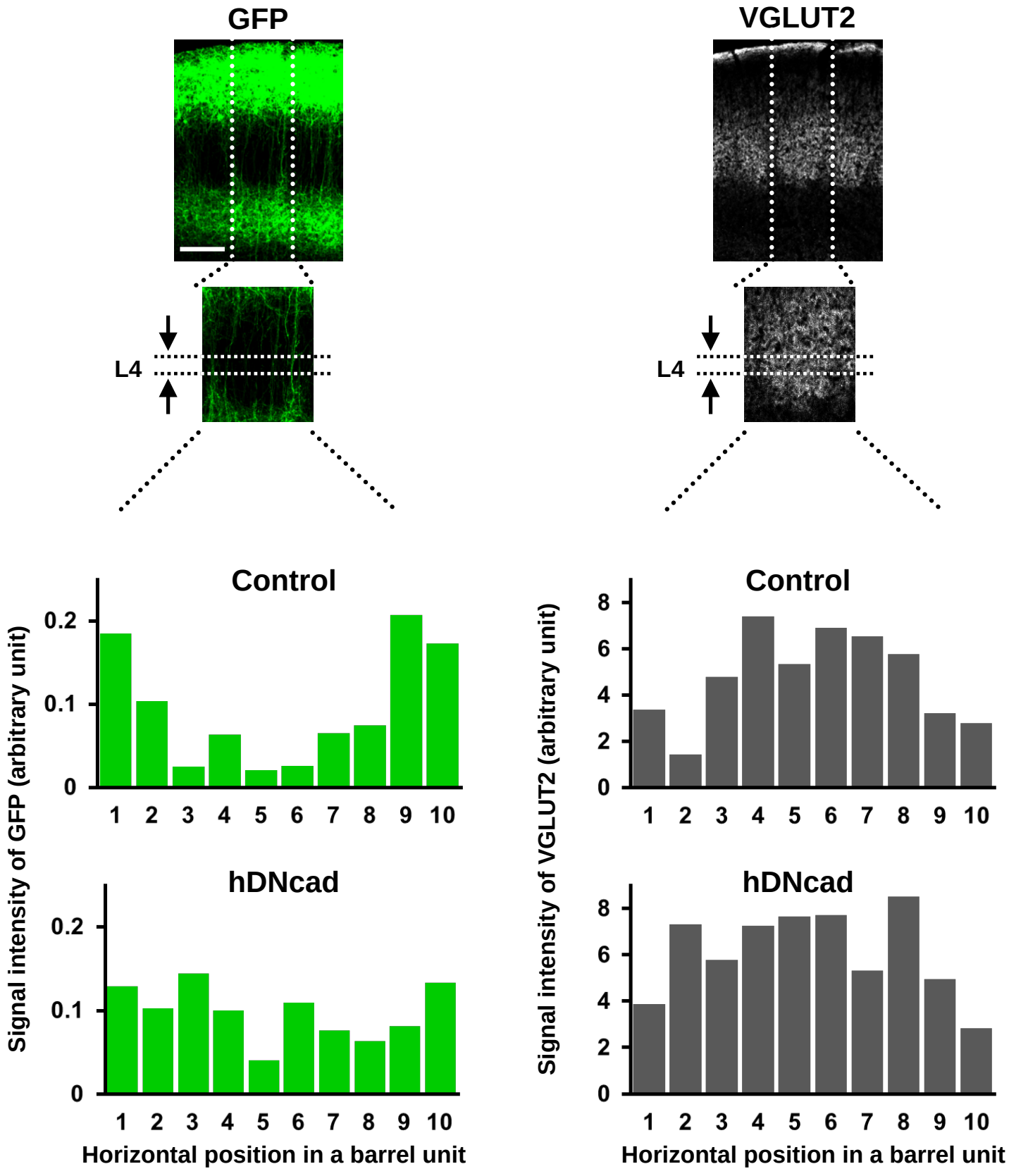

Supplementary Figure3

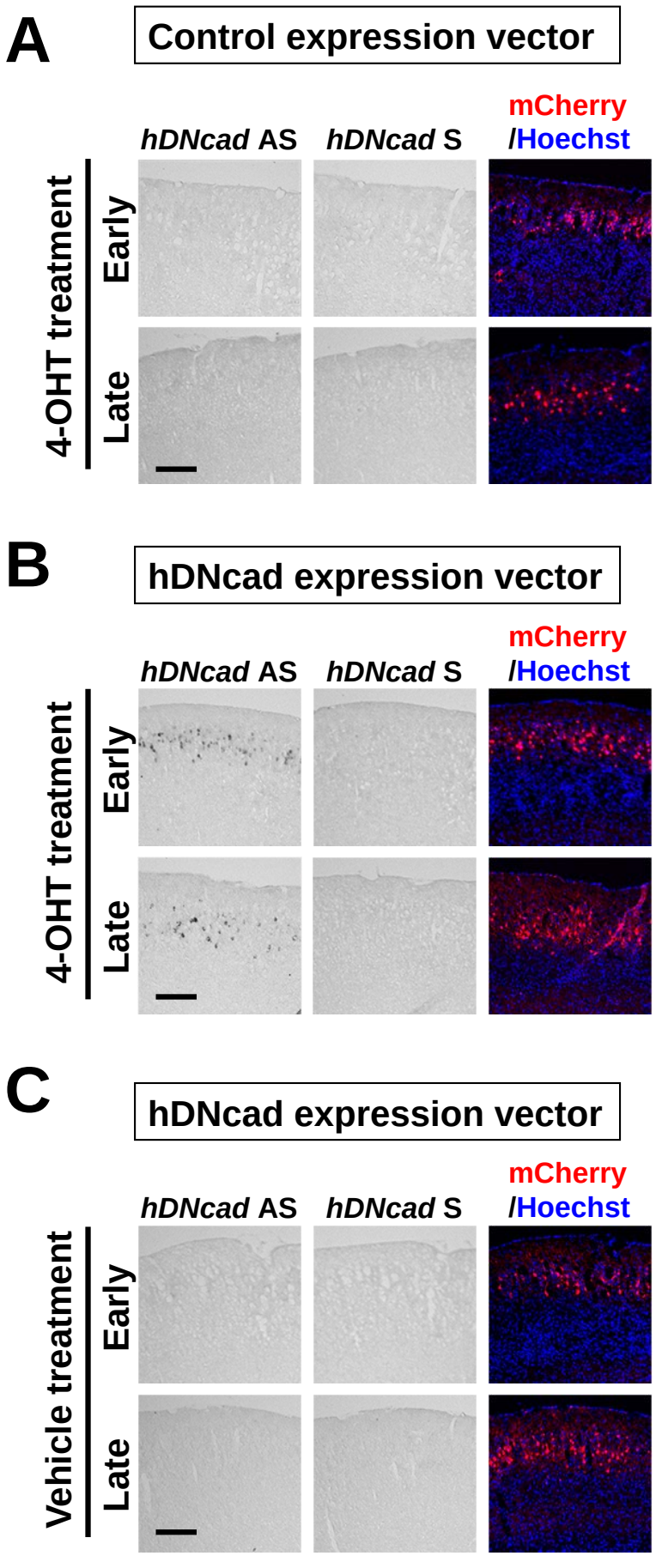

Supplementary Figure4